On Wiener type filtrations in the single-photon emission computed tomography

Jean-Pol Guillement, Roman Novikov

On Wiener type filtrations in the single-photon emission computed tomography

J.-P. Guillement and R.G. Novikov

CNRS, Laboratoire de Mathématiques Jean Leray (UMR 6629), Université de Nantes, BP 92208, F-44322, Nantes cedex 03, France

E-mail: guillement@math.univ-nantes.fr and novikov@math.univ-nantes.fr

Abstract

For 2D data with Poisson noise we give explicit formulas for the optimal space-invariant Wiener type filter with some a priori geometric restrictions on the window function. Proceeding from this result we (1) explain (in particular) an efficiency of some well-known "1D" (approximately optimal) space-invariant Wiener type filtering scheme (with unknown object power spectrum) in single-photon emission computed tomography (SPECT) and positron emission tomography (PET) imaging based on the classical FBP algorithm (or its iterative use) and (2) propose also an efficient 2D (approximately optimal) space-invariant Wiener type filtration (with unknown object power spectrum) for SPECT imaging based on the generalized FBP algorithm (implementing the explicit formula for the nonuniform attenuation correction) and/or the classical FBP algorithm (used iteratively). An efficient space-variant version of the latter 2D filtration is also announced. Numerical examples illustrating the aforementioned results (in the framework of simulated SPECT imaging) are given.

1. Introduction

In the single-photon emission computed tomography (SPECT) one considers a body containing radioactive isotopes emitting photons. The basic problem of SPECT consists in finding the distribution of these isotopes in the body from the emission data (consisting in the radiation measured outside the body by a family of detectors during some fixed time) and some a priori information concerning the body. Usually this a priori information consists in the photon attenuation coefficient in the points of body, where this coefficient is found in advance by the methods of the transmission computed tomography (under some conditions, this coefficient can be also approximately found directly from the emission data in the frameworks of the "identification" problem). In 2D SPECT, that is when the problem is restricted to a fixed two-dimensional plane Ξ intersecting the body and identified with $\mathbb{R}^2$, the emission data are modeled, in some approximation, as 2D attenuated ray transform with Poisson noise (or, more precisely, as a function p of formula (1.4) given below). Let us remind now related mathematical definitions.

The 2D attenuated ray transformation P_a is defined by the formula

$$P_a f(\gamma) = \int\limits_{\mathbb{R}} \exp\left(-\mathcal{D}a(s\theta^\perp + t\theta, \theta)\right) f(s\theta^\perp + t\theta) dt, \qquad (1.1a)$$

$$\gamma = (s, \theta) \in \mathbb{R} \times \mathbb{S}^1, \quad \theta^\perp = (-\theta_2, \theta_1) \quad \text{for} \quad \theta = (\theta_1, \theta_2) \in \mathbb{S}^1,$$

$$\mathcal{D}a(x,\theta) = \int_0^{+\infty} a(x+t\theta)dt, \quad (x,\theta) \in \mathbb{R}^2 \times \mathbb{S}^1, \tag{1.1b}$$

where a and f are real-valued, sufficiently regular functions on $\mathbb{R}^2$ with sufficient decay at infinity, a is a parameter (the attenuation coefficient), $\mathcal{D}a$ is the divergent beam transform of a, f is a test function. In (1.1a) we interpret $\mathbb{R} \times \mathbb{S}^1$ as the set of all oriented straight lines in $\mathbb{R}^2$. If $\gamma = (s,\theta) \in \mathbb{R} \times \mathbb{S}^1$, then $\gamma = \{x \in \mathbb{R}^2 : \ x = s\theta^\perp + t\theta, \ t \in \mathbb{R}\}$ (modulo orientation) and θ gives the orientation of γ.

In SPECT, $f \geq 0$ is the density of radioactive isotopes, $a \geq 0$ is the linear photon attenuation coefficient of the medium, and (in some approximation) $CP_a f$ is the expected emission data (the expected sinogram), where C is a positive constant depending on detection parameters.

More precisely, saying about the emission data in 2D SPECT, we assume that

$$a(x) \geq 0, \ f(x) \geq 0, \quad \text{for} \ \ x \in \mathbb{R}^2, \ a(x) \equiv 0, \quad f(x) \equiv 0 \ \ \text{for} \ \ |x| \geq R \tag{1.2}$$

and consider in $\mathbb{R} \times \mathbb{S}^1$ a discrete subset of the form

$$\begin{aligned} &\Gamma = \{\gamma_{i,j} = (s_i, \theta(\varphi_j)) : \ s_i = -R + (i-1)\Delta s, \ \varphi_j = (j-1)\Delta\varphi, \\ &\Delta s = 2R/(n_s - 1), \ \Delta\varphi = 2\pi/n_\varphi, \quad i = 1, \dots, n_s, \ j = 1, \dots, n_\varphi\}, \end{aligned} \tag{1.3}$$

where $\theta(\varphi) = (\cos\varphi, \sin\varphi)$, R is the radius of image support of (1.2), n_s, n_φ are sufficiently large natural numbers, and n_φ is even. We say that Γ is a detector set. (Note that $\Gamma \subset \{(s,\theta) \in \mathbb{R} \times \mathbb{S}^1 : \ |s| \leq R\}$, where R is the number of (1.2).)

In 2D SPECT, in some approximation, the emission data consist of a function p on Γ, where

$$\begin{aligned} &p(\gamma) \ \ \text{is a realization of a Poisson variate} \ \ \mathbf{p}(\gamma) \\ &\text{with the mean} \ \ M\mathbf{p}(\gamma) = g(\gamma) = CP_a f(\gamma) \ \ \text{for any} \ \ \gamma \in \Gamma \\ &\text{and all} \ \ \mathbf{p}(\gamma), \ \ \gamma \in \Gamma, \ \ \text{are independent.} \end{aligned} \tag{1.4}$$

In addition, it is assumed that $C = C_1 t$, where t is the detection time per projection and C_1 is independent of t. We say that p of (1.4) is the 2D attenuated ray transform ($CP_a f$ on Γ) with Poisson noise.

For more information concerning the aforementioned basic points of SPECT, see, for example, [NW], [LM], [Br] and references therein.

In the present work we consider the following two problems:

Problem 1.1. Find (as well as possible) g from p, where g and p are the function of (1.4).

Problem 1.2. Find (as well as possible) Cf from the p and a, where f, a and p are the function of (1.2), (1.4) and C is the constant of (1.4).

More precisely, in the present work we develop space-invariant Wiener type filtration approach (of [KDS]) for solving Problem 1.1 and apply this approach to solving Problem 1.2 in the framework of the scheme

$$Cf \approx P_a^{-1} \mathcal{W} p, \tag{1.5}$$

where $\mathcal{W}$ is a filtration for solving Problem 1.1 and P_a^{-1} is an inversion method for P_a for the noiseless case. In particular, for 2D data with Poisson noise we give explicit formulas for the optimal space-invariant Wiener type filter with some a priori geometric restrictions on the window function; see Proposition 3.1 of Section 3. Then (in Section 4), proceeding from this result we (1) explain, in particular, an efficiency of the well-known "1D" (approximately optimal) space-invariant Wiener type filtering scheme of [KDS] (with unknown object power spectrum) in SPECT and PET imaging based on the classical FBP algorithm (or its iterative use) and (2) propose also an efficient 2D (approximately optimal) space-invariant Wiener type filtration $\mathcal{A}^{sym}$ (with unknown object power spectrum) for SPECT imaging based on the generalized FBP algorithm of [Ku], [Na] (implementing the explicit formula of [No] for P_a^{-1} of (1.5)) and/or the classical FBP algorithm (used iteratively). (We do not know whether the filter $\mathcal{A}^{sym}$ in its precise form of Section 4 was mentioned in the literature.)

Actually, in the present work, as P_a^{-1} of (1.5) we use the explicit formula of [No] and the iterative method of [MNOY] (related results are reminded in Section 5).

Numerical examples illustrating the aforementioned results on Problems 1.1 and 1.2 are given in Section 6. In these examples we consider a version of the well-known elliptical chest phantom used for numerical simulations of cardiac SPECT imaging. One can see, in particular, that in these examples the 2D (approximately optimal) space-invariant Wiener type filtration $\mathcal{A}^{sym}$ of Section 4 with the window function given by (4.8), (4.9), (4.12), (4.13) is more efficient (as regards image errors and image bias) than the 2D space-invariant data dependent filtration of [GN1].

Finally, it should be mentioned also that the noise level in the emission data p of (1.4) is not space-invariant and in this respect all space-invariant filtrations are not optimal for Problems 1.1 and 1.2. Space-variant versions of the space-invariant data dependent filtration of [GN1] are constructed in [GN2]. Space-variant versions of the space-invariant Wiener type filtrations considered in the present work are constructed and analyzed in [GN3]. In addition, our simplest space-variant version $\mathcal{A}^{sym}_{l_1,l_2}$ of the aforementioned $\mathcal{A}^{sym}$ is already mentioned and illustrated numerically in Subsection 6.4. In particular, our best (iterative) reconstruction Cf_3 (of (6.25)) is obtained using namely $\mathcal{A}^{sym}_{l_1,l_2}$ (for $l_1 = l_2 = 8$). To our knowledge no complete generalization to the space-variant case of the filtration approach of [KDS] was presented in the literature before the present work.

2. Frequency domain form of space invariant filters

Consider the functions p and g of (1.4). Suppose that

$$g(s_i, \theta(\varphi_j)) \equiv 0, \quad \text{if} \quad ||s_i| - R| < L, \tag{2.1}$$

where $\Delta s << L$, where s_i, φ_j, R and Δs are the numbers of (1.3). Then p and g of (1.4) can be considered as functions on a discrete torus identified with Γ. Note that Γ of (1.3) can be identified with

$$I = \{(i_1, i_2) \in \mathbb{Z}^2 : \ 0 \le i_1 \le n_s - 1, \ \ 0 \le i_2 \le n_\varphi - 1\}. \tag{2.2}$$

Let us suppose that n_φ and n_s of (1.3), (2.2) are even. Let

$$\hat{I} = \{(j_1, j_2) \in \mathbb{Z}^2 : \ -\frac{n_s}{2} \le j_1 \le \frac{n_s}{2} - 1, \ \ -\frac{n_\varphi}{2} \le j_2 \le \frac{n_\varphi}{2} - 1\}. \tag{2.3}$$

Let

$$\|q\|_{L^\alpha(\Gamma')} = (\Delta s \Delta\varphi \sum_{\gamma\in\Gamma'} |q(\gamma)|^\alpha)^{1/\alpha}, \tag{2.4}$$

$$\begin{aligned} \|u\|_{L^\alpha(I')} &= (\sum_{(i_1,i_2)\in I'} |u(i_1,i_2)|^\alpha)^{1/\alpha}, \\ \|\hat{u}\|_{L^\alpha(\hat{I}')} &= (\sum_{(j_1,j_2)\in \hat{I}'} |\hat{u}(j_1,j_2)|^\alpha)^{1/\alpha}, \end{aligned} \tag{2.5}$$

where q, u, $\hat{u}$ are test functions on $\Gamma' \subseteq \Gamma$, $I' \subseteq I$, $\hat{I}' \subseteq \hat{I}$, respectively, $\alpha \in \mathbb{N}$.

Let F denote the 2D discrete Fourier transformation

$$\begin{aligned} &F:\ L^2(I) \to L^2(\hat{I}),\ (Fu)(j_1,j_2) = \\ &\frac{1}{\sqrt{n_s n_\varphi}} \sum_{(i_1,i_2)\in I} u(i_1,i_2)\times \\ &\exp\left(-2\pi i\left(\frac{j_1 i_1}{n_s} + \frac{j_2 i_2}{n_\varphi}\right)\right),\quad (j_1,j_2)\in\hat{I},\quad i=\sqrt{-1}, \end{aligned} \tag{2.6}$$

where u is a test function on I.

To use $F:\ L^2(I) \to L^2(\hat{I})$ and $F^{-1}:\ L^2(\hat{I}) \to L^2(I)$ for filtering p of (1.4) we use also, in particular, the identification operators

$$\Lambda:\ L^2(\Gamma) \to L^2(I),\quad (\Lambda q)(i_1,i_2) = q(\gamma_{i_1,i_2}),\quad (i_1,i_2)\in I, \tag{2.7}$$

$$\Lambda^{-1}:\ L^2(I) \to L^2(\Gamma),\quad (\Lambda u)(\gamma_{i_1,i_2}) = u(i_1,i_2),\quad (i_1,i_2)\in I, \tag{2.8}$$

where $\gamma_{i,j}$ is defined in (1.3), q and u are test functions on Γ and I, respectively.

A general linear space invariant filtration in $L^2(\Gamma)$, where Γ is considered as a discrete torus, can be written in the form

$$\mathcal{W}:\ L^2(\Gamma) \to L^2(\Gamma),\quad \mathcal{W} = \Lambda^{-1} W \Lambda, \tag{2.9}$$

where

$$W:\ L^2(I) \to L^2(I),\quad W = F^{-1}\hat{W}F, \tag{2.10}$$

$$\hat{W}:\ L^2(\hat{I}) \to L^2(\hat{I}),\quad (\hat{W}\hat{u})(j) = \hat{W}(j)\hat{u}(j),\quad j=(j_1,j_2)\in\hat{I}, \tag{2.11}$$

where F, Λ, Λ^{-1} are defined in (2.6)-(2.8),

$$\hat{W}(j) \text{ is a real bounded function of } j\in\hat{I}, \tag{2.12a}$$

$$\begin{aligned} &\hat{W}(-j) = \hat{W}(j) \text{ for } \hat{W} \text{ considered as a periodic} \\ &\text{function on } \mathbb{Z}^2 \text{ with the fundamental domain } \hat{I}, \end{aligned} \tag{2.12b}$$

and $\hat{u}$ is a test function. Here the multiplication operator $\hat{W}$ of (2.11) is the frequency domain form of the space invariant filtrations $\mathcal{W}$ and W of (2.9), (2.10). In addition, $\hat{W}(j)$ is the related window function.

Note also that in the simplest space-invariant data independent schemes for filtering p of (1.4) the window function $\hat{W}$ of (2.12) is given by

$$\hat{W}(j) = \hat{w}_1\big(\frac{2j_1}{\omega_1 n_s}\big)\hat{w}_2\big(\frac{2j_2}{\omega_2 n_\varphi}\big), \quad j = (j_1, j_2) \in \hat{I}, \quad \omega_1 > 0,\ \omega_2 > 0, \tag{2.13}$$

where $\hat{w}_1(s)$, $\hat{w}_2(s)$ are real-valued functions of s such that

$$\begin{aligned} &\hat{w}_i(s) = \hat{w}_i(-s), \quad s \in \mathbb{R}, \\ &\lim_{s\to 0} \hat{w}_i(s) = \hat{w}_i(0) = 1, \quad \hat{w}_i(s) \equiv 0 \ \text{ for } \ |s| > 1, \\ &\hat{w}_i(s_1) \geq \hat{w}_i(s_2) \ \text{ for } \ |s_1| \leq |s_2|, \end{aligned} \tag{2.14}$$

where $i \in \{1, 2\}$. Here $\vec{\omega} = (\omega_1, \omega_2)$ is the filtration parameter (and it is usually assumed that $0 < \omega_i \leq 1$, $i \in \{1, 2\}$).

3. Optimal Wiener filter and its restrictedly optimal analogs

Suppose that:

$$g \ \text{ is some nonnegative function on } \ \Gamma \ \text{ (and } \ g \not\equiv 0), \tag{3.1a}$$

$$\begin{aligned} &\mathbf{p}(\gamma) \ \text{ is a Poisson variate with the mean } \ M\mathbf{p}(\gamma) = g(\gamma),\ \gamma \in \Gamma, \\ &\text{and all } \ p(\gamma),\ \gamma \in \Gamma, \ \text{ are independent,} \end{aligned} \tag{3.1b}$$

$$p \ \text{ is a realization of } \ \mathbf{p} \ \text{ on } \ \Gamma. \tag{3.1c}$$

Let $\mathcal{W}$ denote a filter of the form (2.9)-(2.12). Then it is well-known (see [GB], [KDS]) that the mean

$$\mu(\mathcal{W}, g) = M\|\mathcal{W}\mathbf{p} - g\|^2_{L^2(\Gamma)} \tag{3.2}$$

is minimal with respect to $\mathcal{W}$ if and only if the window function $\hat{W}(j)$ of (2.11), (2.12) is given by

$$\hat{W}(j) = \hat{W}^{opt}_g(j) \stackrel{\text{def}}{=} \frac{|\hat{g}(j)|^2}{|\hat{g}(j)|^2 + (n_s n_\varphi)^{-1/2}\hat{g}(0)}, \quad j = (j_1, j_2) \in \hat{I}, \tag{3.3}$$

where $\hat{g} = F\Lambda g$ (with F and Λ defined by (2.6), (2.7)). Note that results of such a type go back to [W] and, therefore, the filter $\mathcal{W}$ for p of (3.1), where the window function $\hat{W}$ of (2.11), (2.12) is given by (3.3), is usually referred (see, for example, [KDS], [C] as an optimal Wiener filter.

Note that an obvious obstacle for a direct use of the aforementioned optimal Wiener filter for solving Problem 1.1 consists in the fact that the window $\hat{W}_g$ of (3.3) is given in terms of g which is an unknown of Problem 1.1.

Below in this section, we generalize the "optimal" formula (3.3) to the case of some a priori geometric restrictions on the window function. In some cases such restrictions

are rather natural and satisfactory and (that is the key point) result in "regularized" optimal filters which are much more appropriate for the case with unknown $|\hat{g}|$ (than the initial optimal filter with $\hat{W}$ given by (3.3)). Note that applications of restrictedly optimal Wiener type filters (of this section) to Problem 1.1 involve also approximations considered in Section 4.

Let $S_1, \dots, S_{n^*}$ be subsets of $\hat{I}$ such that

$$\hat{I} = \cup_{\alpha=1}^{n^*} S_\alpha, \quad \text{each} \quad S_\alpha \neq \emptyset, \; S_\alpha \cap S_\beta = \emptyset \;\; \text{if} \;\; \alpha \neq \beta, \tag{3.4a}$$

$$-S_\alpha = S_{\beta(\alpha)} \;\; (\text{in} \;\; \mathbb{Z}^2 \;\; \text{factorized to} \;\; \hat{I}) \;\; \text{for each} \; S_\alpha. \tag{3.4b}$$

Now we consider the problem of finding $\mathcal{W}$ of the form (2.9)-(2.12) such that $\mu(\mathcal{W}, g)$ of (3.2) is minimal for fixed g of (3.1) under the restrictions that

$$\hat{W} \;\; \text{is constant on each fixed} \;\; S_\alpha, \quad \alpha = 1, \dots, n^*, \tag{3.5}$$

where $\hat{W}$ is the window function of $\mathcal{W}$. This problem is solved in the next proposition:

Proposition 3.1. *Let g and $\mathbf{p}$ be defined as in* (3.1a), (3.1b). *Let $\mathcal{W}$ denote a filter of the form* (2.9)-(2.12) *with a priori restrictions* (3.5) *on its window function $\hat{W}$, where $S_1, \dots, S_{n^*}$ satisfy* (3.4). *Then $\mu(\mathcal{W}, g)$ of* (3.2) *is minimal with respect to $\mathcal{W}$ if and only if*

$$\hat{W}(j) = \hat{W}_g^{r.o.}(j) \stackrel{\text{def}}{=} \frac{\Sigma_{g,\alpha(j)}}{\Sigma_{g,\alpha(j)} + (n_s n_\varphi)^{-1/2} \hat{g}(0)}, \quad j \in \hat{I}, \tag{3.6}$$

$$\Sigma_{g,\alpha(j)} \stackrel{\text{def}}{=} \frac{1}{|S_{\alpha(j)}|} \sum_{i \in S_{\alpha(j)}} |\hat{g}(i)|^2, \quad j \in \hat{I}, \tag{3.7}$$

where $\hat{g} = F\Lambda g$ (with F and Λ defined by (2.6), (2.7)), *$\alpha(j)$ denotes α such that $j \in S_\alpha$ and $|S_\alpha|$ denotes the number of elements in S_α.*

Proof of Proposition 3.1. Due to (3.2),(2.9)-(2.12) and the property

$$\|\Lambda^{-1} F^{-1} \hat{u}\|^2_{L^2(\Gamma)} = \Delta s \Delta\varphi \|\hat{u}\|^2_{L^2(\hat{I})}, \quad \hat{u} \in L^2(\hat{I}), \tag{3.8}$$

we have that

$$\mu(\mathcal{W}, g) = \Delta s \Delta\varphi M \|\hat{W}\hat{\mathbf{p}} - \hat{g}\|^2_{L^2(\hat{I})}, \tag{3.9}$$

where $\hat{\mathbf{p}} = F\Lambda\mathbf{p}$, $\hat{g} = F\Lambda g$. Further,

$$\begin{aligned} &M\|\hat{W}\hat{\mathbf{p}} - \hat{g}\|^2_{L^2(\hat{I})} \stackrel{(2.5),(3.4a)}{=} M \sum_{\alpha=1}^{n^*} \|\hat{W}\hat{\mathbf{p}} - \hat{g}\|^2_{L^2(S_\alpha)} = \\ &\sum_{\alpha=1}^{n^*} M\|\hat{W}\hat{\mathbf{p}} - \hat{g}\|^2_{L^2(S_\alpha)} \stackrel{(3.5)}{=} \sum_{\alpha=1}^{n^*} M\|\hat{w}_\alpha \hat{\mathbf{p}} - \hat{g}\|^2_{L^2(S_\alpha)}, \end{aligned} \tag{3.10}$$

where $\hat{w}_\alpha$ are real constants such that

$$\hat{W} \equiv \hat{w}_\alpha \;\; \text{on each fixed} \;\; S_\alpha, \quad \alpha = 1, \dots, n^*. \tag{3.11}$$

Due to (3.9)-(3.11), $\mathcal{W}$ minimizes $\mu(\mathcal{W}, g)$ (for fixed g) if and only if for each α (and fixed g) w_α minimizes

$$\hat{\mu}_\alpha(\hat{w}_\alpha, \hat{g}) \stackrel{\text{def}}{=} M\|\hat{w}_\alpha \hat{\mathbf{p}} - \hat{g}\|^2_{L^2(S_\alpha)}, \quad \alpha = 1, \dots, n^*. \tag{3.12}$$

We have that

$$\begin{aligned} &\hat{\mu}_\alpha(\hat{w}_\alpha, \hat{g}) = M \sum_{j \in S_\alpha} (\hat{w}_\alpha \hat{\mathbf{p}}(j) - \hat{g}(j))\overline{(\hat{w}_\alpha \hat{\mathbf{p}}(j) - \hat{g}(j))} = \\ &\sum_{j \in S_\alpha} M((\hat{w}_\alpha)^2 |\hat{\mathbf{p}}(j)|^2 - \hat{w}_\alpha(\hat{\mathbf{p}}(j)\overline{\hat{g}(j)} + \hat{g}(j)\overline{\hat{\mathbf{p}}(j)}) + |\hat{g}(j)|^2) = \\ &C_{g,\alpha,2}\hat{w}^2_\alpha + C_{g,\alpha,1}\hat{w}_\alpha + C_{g,\alpha,0}, \end{aligned} \tag{3.13}$$

where

$$\begin{aligned} C_{g,\alpha,2} &= \sum_{j \in S_\alpha} M|\hat{\mathbf{p}}(j)|^2, \\ C_{g,\alpha,1} &= -\sum_{j \in S_\alpha} (\overline{\hat{g}(j)} M\hat{\mathbf{p}}(j) + \hat{g}(j) M\overline{\hat{\mathbf{p}}(j)}), \\ C_{g,\alpha,0} &= \sum_{j \in S_\alpha} M|\hat{g}(j)|^2. \end{aligned} \tag{3.14}$$

In addition, $C_{g,\alpha,2} > 0$ due to (3.1a), (3.4a) and (3.17). Therefore, $\hat{\mu}_\alpha(\hat{w}_\alpha, \hat{g})$ is minimal with respect to $\hat{w}_\alpha$ (for fixed g and α) if and only if

$$\hat{w}_\alpha = -\frac{C_{g,\alpha,1}}{2C_{g,\alpha,2}}. \tag{3.15}$$

Formula (3.6) follows from (3.11), (3.15), (3.14) and the formulas

$$M\hat{\mathbf{p}}(j) = \hat{g}(j), \quad j \in \hat{I}, \tag{3.16}$$

$$M|\hat{\mathbf{p}}(j)|^2 = |\hat{g}(j)|^2 + (n_s n_\varphi)^{-1/2}\hat{g}(0), \quad j \in \hat{I}. \tag{3.17}$$

Here (3.16) is rather obvious, whereas (3.17) is, actually, a formula of [GB] (see also [KDS]).

Property (2.12b) for $\hat{W}$ of (3.6) follows from (3.4b), (3.6), (3.7) and the property $|\hat{g}(-j)| = |\hat{g}(j)|$.

Proposition 3.1 is proved.

Note that if

$$S_{\alpha(j)} = \{j\} \ \text{ for any } \ j \in \hat{I}, \tag{3.18}$$

then formula (3.6) of Proposition 3.1 is reduced to formula (3.3).

Note that Proposition 3.1 admits the following generalization:

Proposition 3.1*. *Let all assumptions of Proposition 3.1 be valid except* (3.1a), (3.1b) *which are relaxed now to the assumptions that*

$$g \ \textit{ is a real function on } \ \Gamma \ \ (\textit{and } \ g \not\equiv 0), \tag{3.19a}$$

$$\begin{aligned} &p(\gamma) \text{ is a real variate with the mean } M\mathbf{p}(\gamma) = g(\gamma),\ \gamma \in \Gamma, \\ &\text{and all } \mathbf{p}(\gamma),\ \gamma \in \Gamma, \text{ are independent (and } D\mathbf{p} = M(\mathbf{p} - M\mathbf{p})^2 \not\equiv 0). \end{aligned} \tag{3.19b}$$

Then $\mu(\mathcal{W}, g)$ of (3.2) *is minimal with respect to $\mathcal{W}$ if and only if*

$$\hat{W}(j) = \hat{W}_g^{r.o.}(j) \stackrel{\text{def}}{=} \frac{\Sigma_{g,\alpha(j)}}{\Sigma_{g,\alpha(j)} + (n_s n_\varphi)^{-1/2}\widehat{D\mathbf{p}}(0)},\ j \in \hat{I}, \tag{3.20}$$

where $\Sigma_{g,\alpha(j)}$ is defined by (3.7), $\widehat{D\mathbf{p}} = F\Lambda(D\mathbf{p})$.

Proposition 3.1* is proved by repeating the proof of Proposition 3.1, where instead of (3.17) we use now the formula

$$M|\hat{\mathbf{p}}(j)|^2 = |\hat{g}(j)|^2 + (n_s n_\varphi)^{-1/2}\widehat{D\mathbf{p}}(0),\ j \in \hat{I}. \tag{3.21}$$

Note that (3.21) follows from the definition $\hat{\mathbf{p}} = F\Lambda\mathbf{p}$ (with F and Λ defined by (2.6), (2.7)) and the formulas

$$M|\xi|^2 = D\xi + |M\xi|^2, \tag{3.22}$$

$$D(c_1\xi_1 + c_2\xi_2) = |c_1|^2 D\xi_1 + |c_2|^2 D\xi_2, \tag{3.23}$$

where ξ is a complex-valued variate, $D\xi = M|\xi - M\xi|^2$, c_1 and c_2 are complex constants, ξ_1 and ξ_2 are independent complex-valued variates.

Note, finally, that Propositions 3.1 and 3.1* admit straightforward generalizations to the case of any dimension (and, in particular, to the 3D case).

4. Approximations to the Wiener optimal filter and to its restrictedly optimal analogs

To apply the Wiener optimal filter to Problem 1.1 one needs to express approximately the window $\hat{W}_g^{opt}$ of (3.2) in terms of the data p of (1.4), (3.1c). To construct such approximations one can proceed from formulas (3.16), (3.17). In view of (3.3), (3.16), (3.17), the simplest approximation to $\hat{W}_g^{opt}$ is given by (see, for example, [KDS], [C]):

$$\hat{W}_g^{opt}(j) \approx \hat{A}_p^{simp}(j),\ \ j \in \hat{I}, \tag{4.1}$$

where

$$\begin{aligned} &\hat{A}_p^{simp}(j) = \frac{|\hat{p}(j)|^2 - (n_s n_\varphi)^{-1/2}\hat{p}(0)}{|\hat{p}(j)|^2} \ \text{ if } \ |\hat{p}(j)|^2 - (n_s n_\varphi)^{-1/2}\hat{p}(0) > 0, \\ &\hat{A}_p^{simp}(j) = 0 \ \text{ if } \ |\hat{p}(j)|^2 - (n_s n_\varphi)^{-1/2}\hat{p}(0) \le 0, \end{aligned} \tag{4.2}$$

where $\hat{p} = F\Lambda p$ (with F, Λ defined by (2.6), (2.7)).

Note that $\hat{p}(j)$ is a good approximation to $\hat{g}(j)$, $|\hat{p}(j)|^2$ is a good approximation to $|\hat{g}(j)|^2 + (n_s n_\varphi)^{-1/2}\hat{g}(0)$ and $\hat{A}_p^0(j)$ is a good approximation to $\hat{W}_g^0(j)$ if

$$|\hat{g}(j)| \gg ((n_s n_\varphi)^{-1/2}\hat{g}(0))^{1/2} \ \text{ for fixed } \ j \in \hat{I}. \tag{4.3}$$

This statement follows from formulas (3.16), (3.17) and their corollary that

$$D\hat{\mathbf{p}}(j) = (n_s n_\varphi)^{-1/2}\hat{g}(0), \quad j \in \hat{I}, \tag{4.4}$$

the Chebyshev inequality written in the form

$$Prob\,\{|\xi - M\xi| \le \varepsilon |M\xi|\} \ge 1 - \frac{D\xi}{\varepsilon^2 |M\xi|^2}, \tag{4.5}$$

where $D\xi = M|\xi - M\xi|^2$, and the formulas

$$\begin{aligned} &|\xi|^2 - M|\xi|^2 = |\xi|^2 - |M\xi|^2 - D\xi = (|\xi| - |M\xi|)(|\xi| + |M\xi|) - D\xi, \\ &||\xi|^2 - M|\xi|^2| \le |\xi - M\xi|(2|M\xi| + |\xi - M\xi|) + D\xi \quad (\text{for} \quad \xi = \hat{\mathbf{p}}(j)). \end{aligned} \tag{4.6}$$

As a rule, condition (4.3) is satisfied if j is sufficiently close to 0 but is not satisfied otherwise. Therefore, approximation (4.1), (4.2) to the Wiener optimal filter is not very efficient in the framework of applications to Problem 1.1 and 1.2 (numerical examples are given in Section 6) . Actually, more satisfactory approximations to the Wiener optimal filter can be given proceeding from Proposition 3.1 (with appropriate subsets S_α) as follows.

In a similar way with (4.1), (4.2), in view of formulas (3.6), (3.7) (for the optimal window $\hat{W}_g^{r.o.}$ with a priori restrictions (3.5)) and formulas (3.16), (3.17) (for $M\mathbf{p}$ and $M|\mathbf{p}|^2$) we have that

$$\hat{W}_g^{r.o.}(j) \approx \hat{A}_p(j), \quad j \in \hat{I}, \tag{4.7}$$

where

$$\begin{aligned} &\hat{A}_p(j) = \frac{\Sigma_{p,\alpha(j)} - (n_s n_\varphi)^{-1/2}\hat{p}(0)}{\Sigma_{p,\alpha(j)}} \quad \text{if} \quad \Sigma_{p,\alpha(j)} - (n_s n_\varphi)^{-1/2}\hat{p}(0) > 0, \\ &\hat{A}_p(j) = 0 \quad \text{if} \quad \Sigma_{p,\alpha(j)} - (n_s n_\varphi)^{-1/2}\hat{p}(0) \le 0, \end{aligned} \tag{4.8}$$

where

$$\Sigma_{p,\alpha(j)} = \frac{1}{|S_{\alpha(j)}|} \sum_{i \in S_{\alpha(j)}} |\hat{p}(j)|^2, \quad j \in \hat{I}, \tag{4.9}$$

where $|S_\alpha|$ denotes the number of elements in S_α, $\hat{p} = F\Lambda p$ (with F, Λ defined by (2.6), (2.7)). Note that if S_α are given by (3.18) then formulas (4.7), (4.8) are reduced to (4.1), (4.2).

The principal advantage of the approximation (4.7), (4.8) in comparison with (4.1), (4.2) consists in the fact that if

$$|S_{\alpha(j)}| \quad \text{is great enough in comparison with} \quad |j| \quad \text{for fixed} \quad j \in \hat{I}, \tag{4.10}$$

where $|j|$ is the distance from j to the origin 0 of $\hat{I}$ in an appropriate norm, then (because of averaging in (3.7), (4.9)) $\Sigma_{p,\alpha(j)}$ is a much better approximation to $\Sigma_{g,\alpha(j)} + (n_s n_\varphi)^{-1/2}\hat{g}(0)$

than $|\hat{p}(j)|^2$ to $|\hat{g}(j)|^2 + (n_s n_\varphi)^{-1/2}\hat{g}(0)$ and, as a corollary, $\hat{A}_p(j)$ is a much better approximation to $\hat{W}_g^{r.o.}(j)$ than $\hat{A}_p^{simp}(j)$ to $\hat{W}_g^{opt}(j)$. Moreover, for appropriate subsets S_α it turns out that $\hat{A}_p$ (of (4.8)) is, actually a considerably better approximation to $\hat{W}_g^{opt}$ (of (3.3)) in the framework of applications to Problems 1.1 and 1.2 than A_p^{simp} (of (4.2)).

In particular, window functions as $\hat{A}_p$ of (4.8) for

$$S_{\alpha(j)} = \{z = (z_1, z_2) \in \hat{I} : \ z_1 = j_1\} \ \ \forall\ j = (j_1, j_2) \in \hat{I} \tag{4.11}$$

are actually considered in the literature going back to [KDS] as rather satisfactory approximations to optimal window functions as $\hat{W}_g^{opt}$ in the framework of SPECT and PET imaging based on the classical FBP algorithm or its iterative use (see, for example, [SKC], [BCB], [C]).

Note that $\hat{A}_p$ of (4.8) with S_α given by (4.11) is not very interesting as an approximation to $\hat{W}_g^{opt}$ of (3.3) in the framework of pure applications to Problem 1.1. The reason is that the subsets S_α of (4.11) are not symmetric with respect to the indices z_1 and z_2 on $\hat{I}$ and, therefore, the related space-invariant filter is not symmetric with respect to s and φ variables on Γ. More precisely, due to (4.11) the window function $\hat{W}(j) \stackrel{\text{def}}{=} \hat{A}_p(j)$, $j = (j_1, j_2)$, is independent of j_2 and, therefore, the filter $\mathcal{W}$ of (2.9)-(2.11) with such a window does not filtrate at all with respect to the angle variable φ on Γ. However, the classical FBP algorithm is not very sensitive to stochastic noise in the angle-direction of projections. This together with Proposition 3.1 and property (4.10) for S_α of (4.11) is our explanation of the fact that the filter $\mathcal{W}$ of (2.9)-(2.11) with $\hat{W} = \hat{A}_p$ defined by (4.8), (4.9), (4.11) is rather efficient (in the class of space-invariant filters) in the framework of applications to Problem 1.2 via (1.5) with P_a^{-1} based on iterations of the classical FBP algorithm (see Section 6 for numerical illustration).

To propose adequate $\hat{W}_g^{r.o.}$ and $\hat{A}_p$ (of (3.6), (3.7), (4.8), (4.9)) in the framework of applications to Problem 1.1 and, further, to Problem 1.2 via (1.5) with P_a^{-1} consisting in the generalized FBP algorithm (implementing the explicit formula of [No]) and/or the classical FBP algorithm (used iteratively), see Section 5, we consider the subsets S_α defined as follows:

$$S_\alpha = \{z = (z_1, z_2) \in \hat{I} : \ \tau_{\alpha-1} \le \max\big(|z_1|, \big|\frac{n_s}{n_\varphi} z_2\big|\big) < \tau_\alpha\},\ \alpha = 1, \dots, n^*, \tag{4.12}$$

where $\tau_0, \dots, \tau_{n^*}$ are some appropriate fixed real numbers such that $\tau_0 = 0$, $\tau_{\alpha-1} < \tau_\alpha$ (and $S_\alpha \neq \emptyset$), $\alpha = 1, \dots, n^*$, $\tau_{n^*} = (n_s + 1)/2$ and where we assume that $n_\varphi \le n_s$. Actually, in the numerical examples of present work we assume that $n_\varphi = n_s$ and

$$\tau_0 = 0,\ \tau_\alpha = 1/2 + \alpha, \quad \text{for} \quad \alpha = 1, \dots, n^*, \quad n^* = n_s/2 = n_\varphi/2. \tag{4.13}$$

One can see that the subsets S_α of (4.12), (4.13) are rather symmetric with respect to the indices z_1 and z_2 on $\hat{I}$ in contrast with the subsets S_α of (4.11). As a result $\hat{A}_p$ of (4.8), (4.9) with S_α of (4.12), (4.13) is also of interest as an approximation to $\hat{W}_g^{opt}$ of (3.3) even in the framework of pure applications to Problem 1.1.

In addition, in the framework of further applications to Problem 1.2 via (1.5) (even with P_a^{-1} consisting in the classical FBP algorithm used iteratively) the symmetric $\hat{A}_p$ of (4.8), (4.9), (4.12), (4.13) gives also considerably better results than "1D" $\hat{A}_p$ of (4.8), (4.9), (4.11). Numerical examples illustrating the filter $\mathcal{W}$ of (2.9)-(2.11) with data dependent $\hat{W} = \hat{A}_p$ defined by (4.8), (4.9), (4.12), (4.13) in the framework of applications to Problems 1.1 and 1.2 are given in Section 6. An efficiency of this filter (in the class of space-invariant filters) in the framework of these applications is explained by Proposition 3.1, property (4.10) and adequate geometry of the subsets S_α of (4.12), (4.13).

Finally, note that subsets S_α (arising in (3.6), (3.7), (4.8), (4.9)) with geometry even more appropriate for applications to Problems 1.1 and 1.2 than in (4.12), (4.13) can be constructed proceeding from the result (see [RL], [MN], [GouNol], [GN2] and figure 2(b) of the present paper) that the Fourier transform $\hat{g} = F\Lambda g$, where g is the function of (1.4), is supported mainly in some rather specific domain (of bowtie shape) dependent on f and a. However, we will not develop this issue in the present work.

5. Reconstruction of Cf from CP_af and a

First, we consider the following explicit inversion formula

$$Cf = \mathcal{N}_a g, \tag{5.1}$$

where $g = CP_af$,

$$\mathcal{N}_a q(x) = \frac{1}{4\pi}\left(-\frac{\partial}{\partial x_1}\int\limits_{\mathbb{S}^1} K(x,\theta)\theta_2 d\theta + \frac{\partial}{\partial x_2}\int\limits_{\mathbb{S}^1} K(x,\theta)\theta_1 d\theta\right), \tag{5.2a}$$

$$K(x,\theta) = \exp\left[-\mathcal{D}a(x,-\theta)\right]\tilde{q}_\theta(x\theta^\perp), \tag{5.2b}$$

$$\begin{aligned}\tilde{q}_\theta(s) = {}& \exp\big(A_\theta(s)\big)\cos\big(B_\theta(s)\big)\, H\big(\exp\left(A_\theta\right)\cos\left(B_\theta\right) q_\theta\big)(s) + \\ & \exp\big(A_\theta(s)\big)\sin\big(B_\theta(s)\big)\, H\big(\exp\left(A_\theta\right)\sin\left(B_\theta\right) q_\theta\big)(s),\end{aligned} \tag{5.2c}$$

$$A_\theta(s) = \frac{1}{2}Pa(s,\theta), \quad B_\theta(s) = H\, A_\theta(s), \quad q_\theta(s) = q(s,\theta), \tag{5.2d}$$

where q is a test function, $P = P_0$ is the classical two-dimensional ray transformation (i.e. P_0 is defined by (1.1a) with $a \equiv 0$), H is the Hilbert transformation defined by the formula

$$H\, u(s) = \frac{1}{\pi}\, p.v. \int\limits_{\mathbb{R}} \frac{u(t)}{s-t} dt, \tag{5.3}$$

where u is a test function, $x = (x_1, x_2) \in \mathbb{R}^2$, $\theta = (\theta_1, \theta_2) \in \mathbb{S}^1$, $\theta^\perp = (-\theta_2, \theta_1)$, $s \in \mathbb{R}$, $d\theta$ is arc-length measure on the circle $\mathbb{S}^1$.

In a slightly different form (using complex notations) formula (5.1) was obtained in [No]. Some new proofs of this formula were given in [Na] and [BS]. Formula (5.1) was successfully implemented numerically in [Ku] and [Na] via a direct generalization of the (classical) filtered back-projection (FBP) algorithm. However, this generalized FBP algorithm turned out to be less stable, in general, than its classical analogue. Some possibilities

for improving the stability of SPECT imaging based on (5.1), (5.2) with respect to the Poisson noise in the emission data g were proposed, in particular, in [Ku] (preprint version), [GJKNT] and [GN]. Some fast numerical implementation of formula (5.1) was proposed in [BM].

Second, assuming (1.2), we consider the iterative reconstruction method with the following step. If Cf_n is an approximation with the number n to Cf (as an approximation Cf_n may have some negative values) and $g = CP_af$, then we

(1) compute

$$h_n(s,\theta) = (g(s,\theta) + \mu_n)\frac{PCf_n(s,\theta) + \mu_n}{P_aCf_n(s,\theta) + \mu_n} - \mu_n, \tag{5.4}$$

where μ_n is some sufficiently small positive constant depending on P_aCf_n such that $P_aCf_n(s,\theta) + \mu_n > 0$ for $(s,\theta) \in \mathbb{R} \times \mathbb{S}^1$, $P = P_0$ is defined by (1.1a) with $a \equiv 0$,

(2) enforce the conditions

$$0 \le g(s,\theta) \le h_n(s,\theta) \le \exp\left(Pa(s,\theta)\right)g(s,\theta),\ (s,\theta) \in \mathbb{R} \times \mathbb{S}^1, \tag{5.5}$$

and (3) compute

$$Cf_{n+1} = P^{-1}h_n \tag{5.6}$$

using (5.1) with $a \equiv 0$ (i.e. using a variant of the classical FBP algorithm). This step (i.e. the passage from Cf_n to Cf_{n+1} via (5.4)-(5.6)) is a variation of the step of the iterative SPECT reconstruction algorithm of [MNOY] (see also [MIMIKIH] and [GJKNT]). This algorithm (with the step (5.4)-(5.6)) is rather stable or, more precisely, its stability properties with respect to the Poisson noise in the emission data g are comparable with the stability properties of (5.1) for $a \equiv 0$ (i.e. with the stability properties of the classical FBP algorithm).

In the present work we improve the stability of SPECT reconstruction based on (5.1), (5.2) or/and on (5.4)-(5.6) with respect to the Poisson noise in the emission data g by means of approximately optimal space-invariant Wiener type filtrations (with unknown object power spectrum) of Section 4 and one of their space-variant versions (of [GN3]) mentioned in Section 6 (in Subsection 6.4).

Actually, in the present work we consider, mainly, the reconstructions Cf_1 and Cf_3, where Cf_1 is reconstructed via (5.1), (5.2) and Cf_2, Cf_3 are obtained proceeding from Cf_1 via (5.4)-(5.6). Actually, the iterations Cf_2 and Cf_3 are rather close to each other, but nevertheless Cf_3 is still somewhat more stable and more properly illustrates stability properties of the classical FBP algorithm used iteratively. This can be considered as a stabilization of (5.1) or as an acceleration of the iterative reconstruction based on (5.4)-(5.6).

6. Numerical examples

6.1. *Preliminary remarks.* In our numerical examples the attenuation map a and the emitter activity f (and all reconstructions of f) are actually considered on

$$\begin{aligned} &X = \{x_{i,j} :\ x_{i,j} = (-R + (i-1)\Delta s, -R + (j-1)\Delta s),\\ &\Delta s = 2R/(n_s - 1),\quad i = 1,\dots,n_s,\ j = 1,\dots,n_s\} \end{aligned} \tag{6.1}$$

(where i, j are used as coordinates on X), the attenuated ray transform $g = CP_a f$ and the noisy emission data p (and all filtrations of p) are considered on Γ defined by (1.3), where R of (6.1) and (1.3) is the radius of image support of (1.2) and $n_s = 128$, $n_\varphi = 128$ in (6.1), (1.3); in addition the 2D discrete Fourier transform $F\Lambda q$ is considered on $\hat{I}$ defined by (2.3) for any q on Γ.

Given f and a on X, we assume that $P_a f$ is defined on Γ and is the numerical realization of (1.1) as in [Ku]. Given a on X and q on Γ, we assume that $\mathcal{N}_a q$ is defined on X and denote the numerical realization of (5.2) as in [Ku], [Na] without any regularization. Given Cf_1 and a on X and g on Γ, we assume that $Cf_m(Cf_1, a, g)$ is defined on X and is obtained numerically proceeding from Cf_1 via (5.4)-(5.6) by $m-1$ steps without any regularization in (5.6) (here we do not assume that $g = CP_a f$).

In our studies we consider also the following two-dimensional images

$$\begin{aligned} M_k\mathcal{W}\mathbf{p} &= \frac{1}{k}\sum_{i=1}^{k}\mathcal{W}p_i, \\ D_k\mathcal{W}\mathbf{p} &= \frac{1}{k}\sum_{i=1}^{k}(\mathcal{W}p_i - M_k\mathcal{W}\mathbf{p})^2, \end{aligned} \tag{6.2}$$

$$\begin{aligned} M_k P_a^{-1}\mathcal{W}\mathbf{p} &= \frac{1}{k}\sum_{i=1}^{k} M_k P_a^{-1}\mathcal{W}p_i, \\ D_k P_a^{-1}\mathcal{W}\mathbf{p} &= \frac{1}{k}\sum_{i=1}^{k}(P_a^{-1}\mathcal{W}p_i - M_k P_a^{-1}\mathcal{W}\mathbf{p})^2, \end{aligned} \tag{6.3}$$

where $\mathcal{W}$ is a fixed filtration method for solving Problem 1.1, $\mathbf{p}$ is the Poisson field of (1.4), $p_1, \ldots, p_k$ are some k independent realizations of $\mathbf{p}$, P_a^{-1} is a fixed inversion method for P_a of (1.1), (1.4) for the noiseless caser. In addition, k is rather great so that $M_k \approx M = M_\infty$, $D_k \approx D = D_\infty$.

Notice that all two-dimensional images of the present work, except the spectrum of projections, are drawn using a linear grayscale, in such a way that the dark gray color represents zero (or negative values, if any) and white corresponds to the maximum value of the imaged function. For the spectrum of projections, a non-linear grayscale was used, because of too great values of the spectrum for small frequencies.

We use also the following notations

$$\zeta(q_2, q_1, \Gamma) = \frac{\|q_2 - q_1\|_{L^2(\Gamma)}}{\|q_1\|_{L^2(\Gamma)}}, \tag{6.4}$$

where q_1, q_2 are test functions on Γ and $\|\cdot\|_{L^2(\Gamma)}$ is defined by (2.4), and

$$\eta(u_1, u_2, X) = \frac{\|u_2 - u_1\|_{L^2(X)}}{\|u_1\|_{L^2(X)}}, \tag{6.5}$$

$$\|u\|_{L^n(X)} = \Delta s\big(\sum_{x\in X} |u(x)|^n\big)^{1/n}, \quad n \in \mathbb{N}, \tag{6.6}$$

where u, u_1, u_2 are test functions on X. Note that for p and g of (1.4) the quantity $\zeta(p, g, \Gamma)$ is the noise level (in the L^2- sense) of p on Γ.

In our studies we consider, in particular, the following numbers

$$\begin{aligned} &e_{1,k}(\mathcal{W}, g) = (M_k(\zeta(\mathcal{W}\mathbf{p}, g, \Gamma))^2)^{1/2} = \big(\frac{1}{k}\sum_{i=1}^{k}(\zeta(\mathcal{W}p_i, g, \Gamma))^2\big)^{1/2}, \\ &b_{1,k}(\mathcal{W}, g) = \zeta(M_k\mathcal{W}\mathbf{p}, g, \Gamma), \\ &d_{1,k}(\mathcal{W}, g) = \frac{\big(\|D_k\mathcal{W}\mathbf{p}\|_{L^1(\Gamma)}\big)^{1/2}}{\|g\|_{L^2(\Gamma)}}, \end{aligned} \tag{6.7}$$

$$\begin{aligned} &e_{2,k}(P_a^{-1}, \mathcal{W}, g) = (M_k(\eta(P_a^{-1}\mathcal{W}\mathbf{p}, P_a^{-1}g, X))^2)^{1/2} = \\ &\big(\frac{1}{k}\sum_{i=1}^{k}(\eta(P_a^{-1}\mathcal{W}p_i, P_a^{-1}g, X))^2\big)^{1/2}, \\ &b_{2,k}(P_a^{-1}, \mathcal{W}, g) = \eta(M_kP_a^{-1}\mathcal{W}\mathbf{p}, P_a^{-1}g, X), \\ &d_{2,k}(P_a^{-1}, \mathcal{W}, g) = \frac{\big(\|D_kP_a^{-1}\mathcal{W}\mathbf{p}\|_{L^1(X)}\big)^{1/2}}{\|P_a^{-1}g\|_{L^2(X)}}, \end{aligned} \tag{6.8}$$

where $\mathcal{W}$, P_a^{-1}, $\mathbf{p}$, $p_1, \ldots, p_k$, $M_k\mathcal{W}\mathbf{p}$, $D_k\mathcal{W}\mathbf{p}$, $M_kP_a^{-1}\mathcal{W}\mathbf{p}$, $D_kP_a^{-1}\mathcal{W}\mathbf{p}$ are the same that in (6.2), (6.3), g is the function of (1.4) and ζ, η, $\|\cdot\|_{L^n(\Gamma)}$, $\|\cdot\|_{L^n(X)}$ are defined in (6.4), (6.5), (2.4), (6.6). One can see that the numbers $e_{1,k}$, $b_{1,k}$, $d_{1,k}$, $e_{2,k}$, $b_{2,k}$, $d_{2,k}$ of (6.7), (6.8) have the following sense:

(1) $e_{1,k}$ is a relative mean error, $b_{1,k}$ is a relative mean bias and $d_{1,k}$ is a relative mean deviation from the mean result (of k tests) for $\mathcal{W}\mathbf{p}$ with fixed g and

(2) $e_{2,k}$ is a relative mean error, $b_{2,k}$ is a relative mean bias and $d_{2,k}$ is a relative mean deviation from the mean result (of k tests) for $P_a^{-1}\mathcal{W}\mathbf{p}$ with fixed g. In addition,

$$(e_{1,k})^2 \approx \mu \tag{6.9}$$

for $e_{1,k}$ of (6.7) and μ of (3.2) (where $\mathcal{W}$ and g are the same that in (6.7)) and for sufficiently great k. Note also that

$$(e_{i,k})^2 \approx (b_{i,k})^2 + (d_{i,k})^2, \quad i = 1, 2, \tag{6.10}$$

for $e_{i,k}$, $b_{i,k}$, $d_{i,k}$, $i = 1, 2$, of (6.7), (6.8) with sufficiently great k.

To compare different filters we consider also the numbers

$$c_{1,k}(\mathcal{W}, g) = \frac{(e_{1,k}(\mathcal{W}, g)b_{1,k}(\mathcal{W}, g))^{1/2}}{|e_{1,k}(Id, g) - e_{1,k}(\mathcal{W}, g)|}, \tag{6.11}$$

$$c_{2,k}(P_a^{-1}, \mathcal{W}, g) = \frac{(e_{2,k}(P_a^{-1}, \mathcal{W}, g)b_{2,k}(P_a^{-1}, \mathcal{W}, g))^{1/2}}{|e_{2,k}(P_a^{-1}, Id, g) - e_{2,k}(P_a^{-1}, \mathcal{W}, g)|}, \tag{6.12}$$

where we use the same notations that in (6.2), (6.3), (6.7), (6.8) and, in addition, Id denotes the identity filter that is $Id(\mathbf{p}) = \mathbf{p}$. We consider $c_{i,k}$ as an error-bias trade-off coefficient between $e_{i,k}$ and $b_{i,k}$, where we take also into account the initial error $e_{i,k}^{initial}$, where $i = 1, 2$, $e_{1,k}^{initial} = e_{1,k}(Id, g)$, $e_{2,k}^{initial} = e_{2,k}(P_a^{-1}, Id, g)$. This trade-off is better if $c_{i,k}$ is smaller.

6.2. Elliptical chest phantom. We consider a version of the elliptical chest phantom (used for numerical simulations of cardiac SPECT imaging; see [HL], [Br], [GN1]). This version is, actually, the same that in [GN1], [GN2] and its description consists in the following:

(1) The major axis of the ellipse representing the body is 30 cm. This phantom is referred further as phantom 1.

(2) The attenuation map is shown in figure 1(a); the attenuation coefficient a is 0.04 cm^{-1} in the lung regions (modeled as two interior ellipses), 0.15 cm^{-1} elsewhere within the body ellipse, and zero outside the body.

(3) The emitter activity f is shown in figure 1(b); f is in the ratio 8:0:1:0 in myocardium (represented as a ring), lungs, elsewhere within the body, and outside the body.

(4) The attenuated ray transform $g = CP_af$ and noisy emission data p of (1.4) are shown in figures 2(a), 2(c). In addition, the constant C was specified by the equation

$$\|g\|_{L^1(\Gamma)}/\|g\|^2_{L^2(\Gamma)} = 0.30 \tag{6.13}$$

in order to have that the noise level $\zeta(p, g, \Gamma) \approx 0.30$ (where ζ is defined by (2.4)). Actually, we have that

$$\zeta(p, g, \Gamma) = 0.298 \tag{6.14}$$

for p shown in figure 2(c).

Figures 2(b), 2(d) show the spectrum $|F\Lambda g|$ and $|F\Lambda p|$.

Figures 3(a)-(d) show the reconstructions

$$Cf_1^0 = \mathcal{N}_a g, \quad Cf_3^0 = Cf(Cf_1^0, a, g) \tag{6.15}$$

(from the noiseless emission data g) and their profiles for $j = 64$.

Figures 4(a)-(d), 5(a)-(d) show the reconstructions

$$Cf_1 = \mathcal{N}_a p, \quad Cf_3 = Cf_3(\mathcal{N}_a p, a, p) \tag{6.16}$$

for p shown in figure 2(c), their profiles for $j = 64$ and the images

$$\begin{aligned} &M_{200}Cf_1 = M_{200}\mathcal{N}_a\mathbf{p}, \quad D_{200}Cf_1 = D_{200}\mathcal{N}_a\mathbf{p}, \\ &M_{200}Cf_3 = M_{200}Cf_3(\mathcal{N}_a\mathbf{p}, a, \mathbf{p}), \quad D_{200}Cf_3 = D_{200}Cf_3(\mathcal{N}_a\mathbf{p}, a, \mathbf{p}) \end{aligned} \tag{6.17}$$

In addition:

$$\eta(Cf_1, Cf_1^0, X) = 1.58, \quad \eta(Cf_3, Cf_3^0, X) = 0.74 \tag{6.18}$$

for Cf_1^0, Cf_3^0, Cf_1, Cf_3 of (6.15), (6.16);

$$e_{2,200} = 1.55, \quad b_{2,200} = 0.11, \quad d_{2,200} = 1.55 \tag{6.19a}$$

for $\mathcal{W} = Id$ (that is $\mathcal{W}(\mathbf{p}) = \mathbf{p}$) and $P_a^{-1} = \mathcal{N}_a$;

$$e_{2,200} = 0.75, \quad b_{2,200} = 0.06, \quad d_{2,200} = 0.75 \tag{6.19b}$$

for $\mathcal{W} = Id$ and

$$P_a^{-1} q = Cf_3(\mathcal{N}_a q, a, q), \tag{6.20}$$

where q is a test function on Γ.

We remind that we use the notations of Subsection 6.1 (and, in particular, i, j are the coordinates on X).

6.3. Illustrations of space-invariant Wiener type filtrations of Sections 3 and 4.

Figures 6-9 show the filtration result $\mathcal{W}p$ and its spectrum $|F\Lambda\mathcal{W}p|$, (for p shown in Figure 2(c)) and also $M_{200}\mathcal{W}\mathbf{p}$ and $D_{200}\mathcal{W}\mathbf{p}$ for $\mathcal{W} = \mathcal{W}_g^{opt}$, $\mathcal{W}_g^{sym}$, $\mathcal{A}^{simp}$, $\mathcal{A}^{sym}$, where $\mathcal{W}_g^{opt}$ is the optimal space-invariant Wiener filter (of Section 3) with the window function given by (3.3), $\mathcal{W}_g^{sym}$ is the restrictedly optimal space-invariant Wiener filter $\mathcal{W}_g^{r.o.}$ (of Proposition 3.1) with the symmetric window function given by (3.6), (3.7), (4.12), (4.13), $\mathcal{A}^{simp}$ is the space-invariant data dependent filter (of Section 4) with the window function defined by (4.2), $\mathcal{A}^{sym}$ is the space-invariant data dependent filter (of Section 4) with the window function defined by (4.8), (4.9), (4.12), (4.13).

We remind that: (1) in $\mathcal{W}_g^{opt}$ and $\mathcal{W}_g^{sym}$ it is assumed that $|\hat{g}|^2$ is known; (2) $\mathcal{A}^{simp}$ is the simplest approximation to $\mathcal{W}_g^{opt}$ for the case when $|\hat{g}|$ is not known; (3) $\mathcal{A}^{sym}$ is a direct approximation to $\mathcal{W}_g^{sym}$ and is a regularized approximation to $\mathcal{W}_g^{opt}$ for the case when $|\hat{g}|$ is not known.

Table 1 shows the number $\zeta = \zeta(\mathcal{W}p, g, \Gamma)$ and $e_{1,200}$, $b_{1,200}$, $d_{1,200}$, $c_{1,k}$ of (6.7), (6.11) for $\mathcal{W} = \mathcal{W}_g^{opt}$, $\mathcal{W}_g^{sym}$, $\mathcal{A}^{simp}$, $\mathcal{A}^{1d}$, $\mathcal{A}^{sym}$ (and for some filters of [GN1], [GN2], [GN3]).

Figures 6-9 and table 1 show that $\mathcal{A}^{simp}$ is not an efficient approximation to $\mathcal{W}_g^{opt}$, whereas $\mathcal{A}^{sym}$ is a very efficient approximation to $\mathcal{W}_g^{sym}$. Moreover, Figures 6, 9 and (related part of) table 1 show that, actually, $\mathcal{A}^{sym}$ is also a rather efficient approximation to $\mathcal{W}_g^{opt}$ in the framework of solving Problem 1.1. We remind that a theoretical explanation of these numerical results was given in Sections 3 and 4.

We do not show the images $\mathcal{W}p$, $|F\Lambda\mathcal{W}p|$, $M_{200}\mathcal{W}\mathbf{p}$, $D_{200}\mathcal{W}\mathbf{p}$ for $\mathcal{W} = \mathcal{W}^{1d}$ and $\mathcal{W} = \mathcal{A}^{1d}$, where $\mathcal{W}_g^{1d}$ is the restrictedly optimal space-invariant Wiener filter $\mathcal{W}_g^{r.o.}$ of Proposition 3.1 with "1d"- window function given by (3.6), (3.7), (4.11) and $\mathcal{A}^{1d}$ is the data dependent approximation to $\mathcal{W}_g^{1d}$ with the window function defined by (4.8), (4.9), (4.11). The reasons are that: (1) it was explained already in Section 4 that $\mathcal{A}^{1d}$ is not interesting in the framework of pure applications to Problem 1.1 and (2) we try to avoid too many images in our paper. Nevertheless, the numbers ζ, $e_{1,200}$, $b_{1,200}$, $d_{1,200}$, $c_{1,200}$ for $\mathcal{W} = \mathcal{A}^{1d}$ are shown in table 1. One can see that the numbers of table 1 for $\mathcal{W} = \mathcal{A}^{sym}$ and $\mathcal{W} = \mathcal{A}^{1d}$ confirm the aforementioned critical remarks concerning $\mathcal{A}^{1d}$.

Figures 10-13 and 16, 17 show the reconstructions

$$Cf_1 = \mathcal{N}_a\mathcal{W}p, \quad Cf_3 = Cf_3(\mathcal{N}_a\mathcal{W}p, a, \mathcal{W}p) \tag{6.21}$$

(from p shown in Figure 2(c)), their profiles for $j = 64$ and

$$\begin{aligned} &M_{200}Cf_1 = M_{200}\mathcal{N}_a\mathcal{W}\mathbf{p}, \quad D_{200}Cf_1 = D_{200}\mathcal{N}_a\mathcal{W}\mathbf{p}, \\ &M_{200}Cf_3 = M_{200}Cf_3(\mathcal{N}_a\mathcal{W}\mathbf{p}, a, \mathcal{W}\mathbf{p}), \quad D_{200}Cf_3 = D_{200}Cf_3(\mathcal{N}_a\mathcal{W}\mathbf{p}, a, \mathcal{W}\mathbf{p}) \end{aligned} \tag{6.22}$$

for $\mathcal{W} = \mathcal{W}_g^{opt}$, $\mathcal{W}_g^{sym}$, $\mathcal{A}^{sym}$. Besides, figures 14, 15 show the reconstruction Cf_3 of (6.21), its profile for $j = 64$ and $M_{200}Cf_3$, $D_{200}Cf_3$ of (6.22) for $\mathcal{W} = \mathcal{A}^{simp}$, $\mathcal{A}^{1d}$.

Table 2 shows the numbers $\eta^{(1)} = \eta(Cf_1, Cf_1^0, X)$ for Cf_1^0, Cf_1 of (6.15), (6.21) and $e_{2,200}^{(1)}$, $b_{2,200}^{(1)}$, $d_{2,200}^{(1)}$, $c_{2,200}^{(1)}$ of (6.8), (6.12) for $\mathcal{W} = \mathcal{W}_g^{opt}$, $\mathcal{W}_g^{sym}$, $\mathcal{A}^{simp}$, $\mathcal{A}^{1d}$, $\mathcal{A}^{sym}$ (and for Φ_1 of [GN1]) and $P_a^{-1} = \mathcal{N}_a$. Table 3 shows the numbers $\eta^{(3)} = \eta(Cf_3, Cf_3^0, X)$ for Cf_3, Cf_3^0 of (6.15), (6.21) and $e_{2,200}^{(3)}$, $b_{2,200}^{(3)}$, $d_{2,200}^{(3)}$, $c_{2,200}^{(3)}$ of (6.8) (6.12) for $\mathcal{W} = \mathcal{W}_g^{opt}$, $\mathcal{W}_g^{sym}$, $\mathcal{A}^{simp}$, $\mathcal{A}^{1d}$, $\mathcal{A}^{sym}$ (and for some filtering schemes of [GN1], [GN2], [GN3]) and P_a^{-1} defined by (6.20).

Figures 10-14, 16, 17 and tables 2, 3 show that $\mathcal{A}^{simp}$ is not an efficient approximation to $\mathcal{W}_g^{opt}$, whereas $\mathcal{A}^{sym}$ is a very efficient approximation to $\mathcal{W}_g^{sym}$ and (moreover) is also a rather efficient approximation to $\mathcal{W}_g^{opt}$ in the framework of applications to Problem 1.2 via reconstructions (6.21) (as well as in the framework of pure applications to Problem 1.1, see figures 6-9, table 1 and related comments). Besides, figures 11, 15 and (related part of) table 3 confirm the well-known numerical result (see [KDS], [SKC], [BCB], [C]) that $\mathcal{A}^{1d}$ is a relatively efficient approximation to $\mathcal{W}_g^{opt}$ in the framework of reconstructions like Cf_3 of (6.21). A theoretical explanation of this numerical result was given in Sections 3 and 4. Nevertheless, figures 15, 17 and (related part of) table 3 show that $\mathcal{A}^{1d}$ is less optimal than $\mathcal{A}^{sym}$ in the framework of the reconstruction Cf_3 of (6.21).

Note also that the reconstruction Cf_1 of (6.21) is not interesting for $\mathcal{W} = \mathcal{A}^{simp}$, $\mathcal{A}^{1d}$ as one can see, in particular, from (related part of) table 2. The reason is that Cf_1 of (6.21) is much more sensitive to residual noise in $\mathcal{W}p$ than Cf_3 and that the residual noise in $\mathcal{A}^{simp}p$ and $\mathcal{A}^{1d}p$ is rather strong. Therefore, to avoid too many images in our paper we do not show Cf_1 of (6.21) and related images for $\mathcal{W} = \mathcal{A}^{simp}$, $\mathcal{A}^{1d}$.

Finally, it makes sense to compare $\mathcal{A}^{sym}$ with the space-invariant data dependent filtration Φ_1 of [GN1]. The window function of Φ_ε is given by (2.13), where

$$\hat{w}_1(s) = \hat{w}_2(s) = \left(\frac{\sin(s)}{s}\right)^2, \quad \omega_1 = \omega_2 = \omega \tag{6.23}$$

and $\omega = \omega(p, \varepsilon)$ is data dependent and is determined from the equation

$$\zeta(p, \Phi_\varepsilon p, \Gamma) \approx \varepsilon \left(\frac{\|p\|_{L^1(\Gamma)}}{\|p\|^2_{L^2(\Gamma)} - \|p\|_{L^1(\Gamma)}}\right)^{1/2} \tag{6.24}$$

for any fixed realization p of $\mathbf{p}$. Actually, there is some similarity in geometric structure of the windows of Φ_1 and $\mathcal{A}^{sym}$. The numbers ζ, $e_{1,200}$, $b_{1,200}$, $d_{1,200}$, $c_{1,200}$ and $\eta^{(i)}$, $e_{2,200}^{(i)}$, $b_{2,200}^{(i)}$, $d_{2,200}^{(i)}$, $c_{2,200}^{(i)}$ $(i = 1, 3)$ for Φ_1 are given in tables 1-3. One can see that these numbers for $\mathcal{A}^{sym}$ are better than for Φ_1. In particular, all bias numbers $b_{1,200}^{(i)}$, $b_{2,200}^{(i)}$ $(i = 1, 3)$ for $\mathcal{A}^{sym}$ are noticeably smaller than for Φ_1. To avoid too many images in our paper we do not show images obtained using Φ_1. Actually, these images confirm that $\mathcal{A}^{sym}$ works better than Φ_1.

6.4. Space-variant filtrations of [GN2] and [GN3]. A space-variant analog $\Phi_{l_1,l_2,\varepsilon}$ of the aforementioned Φ_ε of [GN1] was constructed in [GN2]. In a completely similar way a

space-variant analog $\mathcal{A}^{sym}_{l_1,l_2}$ of $\mathcal{A}^{sym}$ is constructed in [GN3]. The numbers l_1, l_2 mean that this construction involves space-invariant considerations in $l_1 \times l_2$ neighborhood of each $\gamma \in \Gamma$.

Figures 18(a)-(d) show $\mathcal{W}p$, $|F\Lambda\mathcal{W}p|$ (for p shown in figure 2(c)) and $M_{200}\mathcal{W}\mathbf{p}$, $D_{200}\mathcal{W}\mathbf{p}$ for $\mathcal{W} = \mathcal{A}^{sym}_{8,8}$.

Table 1 shows the numbers ζ, $e_{1,200}$, $b_{1,200}$, $d_{1,200}$, $c_{1,200}$ of (6.7), (6.11) for $\mathcal{W} = \mathcal{A}^{sym}_{8,8}$ and $\mathcal{W} = \Phi_{8,8,1}$.

Figures 19(a)-(d) show

$$Cf_3 = Cf_3(\mathcal{N}_a\mathcal{W}_1 p, a, \mathcal{W}p), \tag{6.25}$$

its profile for $j = 64$ and related $M_{200}Cf_3$, $D_{200}Cf_3$ (defined as in (6.22) but with $Cf_3(\mathcal{N}_a\mathcal{W}_1\mathbf{p}, a, \mathcal{W}\mathbf{p})$ in place of $Cf_3(\mathcal{N}_a\mathcal{W}\mathbf{p}, a, \mathcal{W}\mathbf{p})$ for $\mathcal{W}_1 = \mathcal{A}^{sym}$, $\mathcal{W} = \mathcal{A}^{sym}_{8,8}$.

Table 3 shows the numbers $\eta^{(3)} = \eta(Cf_3, Cf_3^0, X)$ for Cf_3^0, Cf_3 of (6.15), (6.25) and $e^{(3)}_{2,200}$, $b^{(3)}_{2,200}$, $d^{(3)}_{2,200}$, $c^{(3)}_{2,200}$ defined as in (6.8) (6.12) with $Cf_3(\mathcal{N}_a\mathcal{W}_1\mathbf{p}, a, \mathcal{W}\mathbf{p})$ in place of $P_a^{-1}\mathcal{W}\mathbf{p}$ and $P_a^{-1}g = Cf_3^0$ of (6.15) for $(\mathcal{W}_1, \mathcal{W}) = (\mathcal{A}^{sym}, \mathcal{A}^{sym}_{8,8})$ and $(\mathcal{W}_1, \mathcal{W}) = (\Phi_1, \Phi_{8,8,1})$.

Note that the high-frequency component of the residual noise in $\mathcal{W}p$ for $\mathcal{W} = \mathcal{A}^{sym}_{8,8}$, $\Phi_{8,8,1}$ is less negligible than for $\mathcal{W} = \mathcal{A}^{sym}$, Φ_1 and that (in general and in our case in particular) $\mathcal{N}_a$ is rather sensitive to this noise component or, more precisely, much more sensitive than the classical FBP algorithm. In addition, $\mathcal{W}_1 p$ is used in (6.25) for the first approximation $Cf_1 = \mathcal{N}_a\mathcal{W}_1 p$ only and $\mathcal{W}p$ is used in (6.25) in the framework of iterations of the classical FBP algorithm only. Therefore, to obtain the best Cf_3 on the level of $e^{(3)}_{2,200}$, we deal with $\mathcal{W}_1 \neq \mathcal{W}$ in (6.25). We do not show $\mathcal{W}p$ for $\mathcal{W} = \Phi_{8,8,1}$ and Cf_3 of (6.25) and related images for $\mathcal{W} = \Phi_{8,8,1}$, $\mathcal{W}_1 = \Phi_1$. The reasons are that: (1) for our phantom (described in subsection 6.2) the aforementioned images are more or less similar to the corresponding images for $\mathcal{W} = \mathcal{A}^{sym}_{8,8}$ and $\mathcal{W}_1 = \mathcal{A}^{sym}$ (actually, $\mathcal{W}p$ and Cf_3 of (6.25) are somewhat more smooth for $\mathcal{W} = \Phi_{8,8,1}$, $\mathcal{W}_1 = \Phi_1$ than for $\mathcal{W} = \mathcal{A}^{sym}_{8,8}$ and $\mathcal{W}_1 = \mathcal{A}^{sym}$) and (2) we try to avoid too many images in our paper.

One can see that in our numerical examples among all filtering schemes mentioned in the present work (1) namely $\mathcal{A}^{sym}_{8,8}$ and $\Phi_{8,8,1}$ have the best trade-off (the least $c_{1,200}$) between the error and bias numbers $e_{1,200}$ and $b_{1,200}$ for the case when $|\hat{g}|$ is not known (see table 1) and (2) namely $\mathcal{W} = \mathcal{A}^{sym}_{8,8}$ (with $\mathcal{W}_1 = \mathcal{A}^{sym}$) has the best trade-off (the least $c^{(3)}_{2,200}$) between the error and bias numbers $e^{(3)}_{2,200}$ and $b^{(3)}_{2,200}$ for the case when $|\hat{g}|$ is not known (see table 3).

For more information on $\Phi_{l_1,l_2,\varepsilon}$ see [GN2]. For more information on $\mathcal{A}^{sym}_{l_1,l_2}$ (and on some other space- variant Wiener type filters for solving Problem 1.1 and Problem 1.2 via (1.5)) see [GN3].

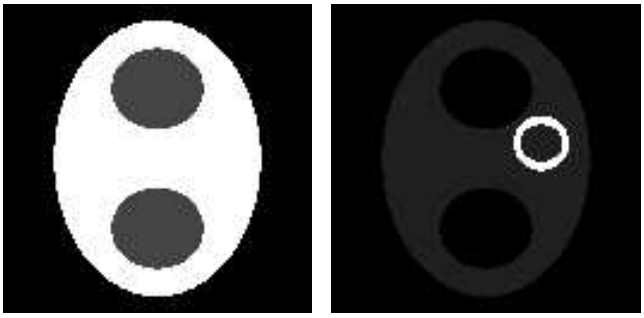

(a) (b)

Figure 1. Attenuation map a (a) and emitter activity f (b).

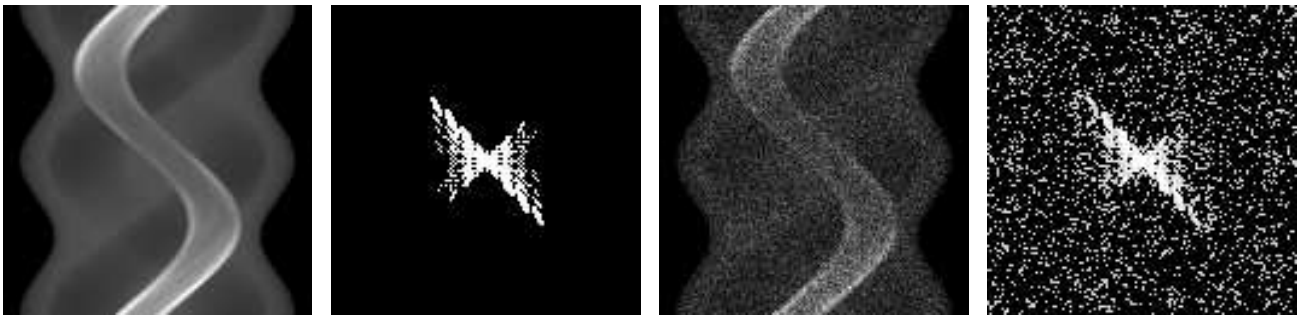

(a) (b) (c) (d)

Figure 2. Noiseless emission data $g = CP_a f$ (a), spectrum $|Fg|$ (b), noisy emission data p (c), spectrum $|Fp|$ (d).

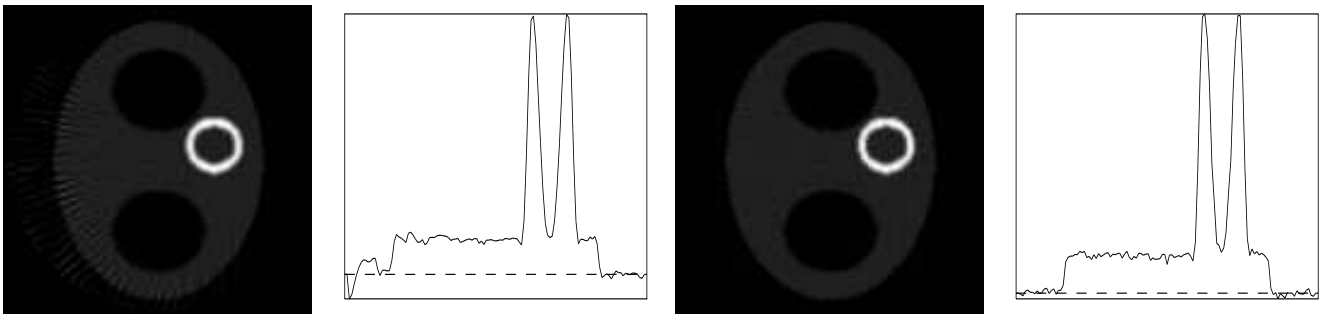

(a) (b) (c) (d)

Figure 3. Reconstructions $Cf_1^0 = \mathcal{N}_a g$ (a) and $Cf_3^0 = Cf_3(Cf_1^0, a, g)$ (c) from the noiseless emission data g, and their profiles for $j = 64$ (b), (d).

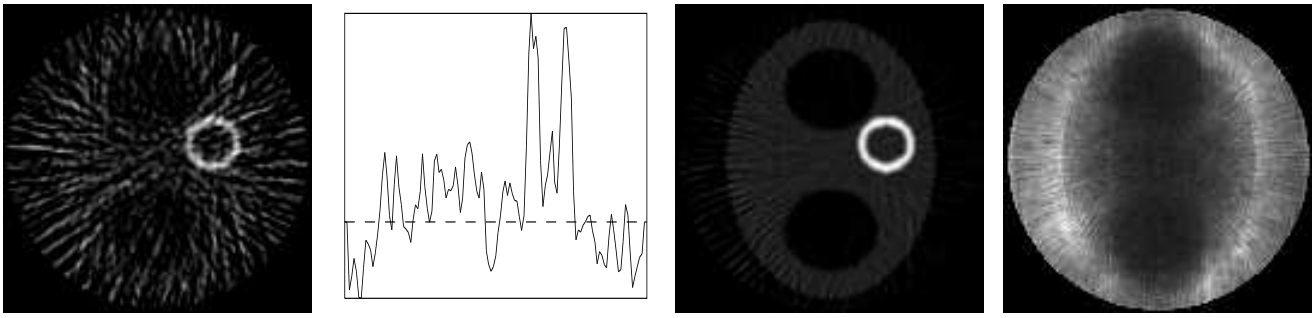

(a) (b) (c) (d)

Figure 4. Reconstruction $Cf_1 = \mathcal{N}_a p$ (a) with its profile for $j = 64$ (b) from the noisy emission data p without any filtration, and related $M_{200}Cf_1$ (c) and $D_{200}Cf_1$ (d).

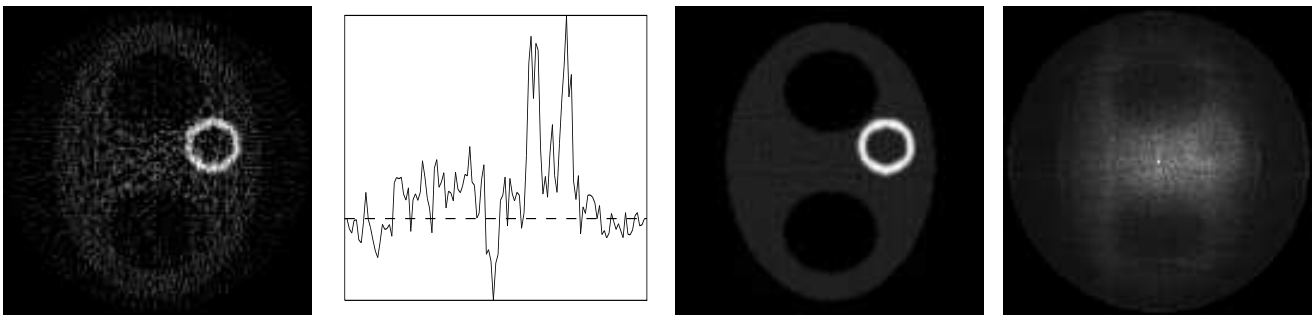

(a) (b) (c) (d)

Figure 5. Reconstruction $Cf_3 = Cf_3(\mathcal{N}_a p, a, p)$ (a) with its profile for $j = 64$ (b) from the noisy emission data p without any filtration, and related $M_{200}Cf_3$ (c) and $D_{200}Cf_3$ (d).

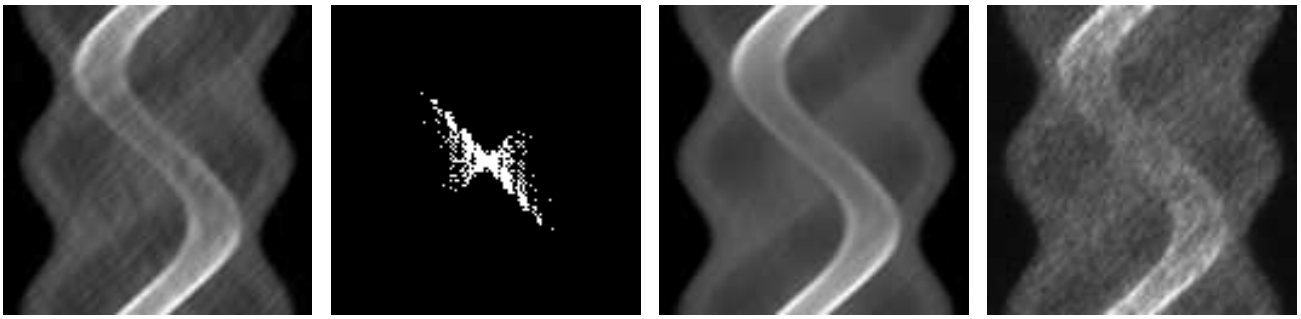

(a) (b) (c) (d)

Figure 6. Filtration result $\mathcal{W}p$ (a), its spectrum $|F\Lambda\mathcal{W}p|$ (b), $M_{200}\mathcal{W}\mathbf{p}$ (c) and $D_{200}\mathcal{W}\mathbf{p}$ (d) for $\mathcal{W} = \mathcal{W}_g^{opt}$.

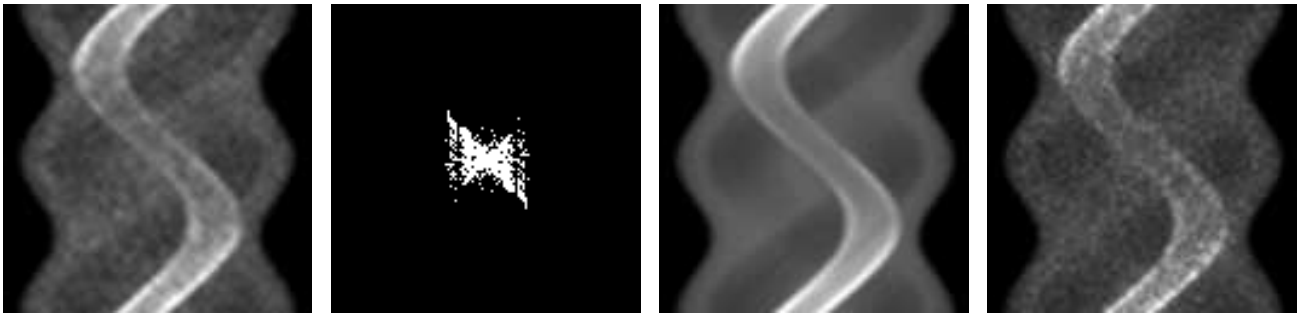

(a) (b) (c) (d)

Figure 7. Filtration result $\mathcal{W}p$ (a), its spectrum $|F\Lambda\mathcal{W}p|$ (b), $M_{200}\mathcal{W}\mathbf{p}$ (c) and $D_{200}\mathcal{W}\mathbf{p}$ (d) for $\mathcal{W} = \mathcal{W}_g^{sym}$.

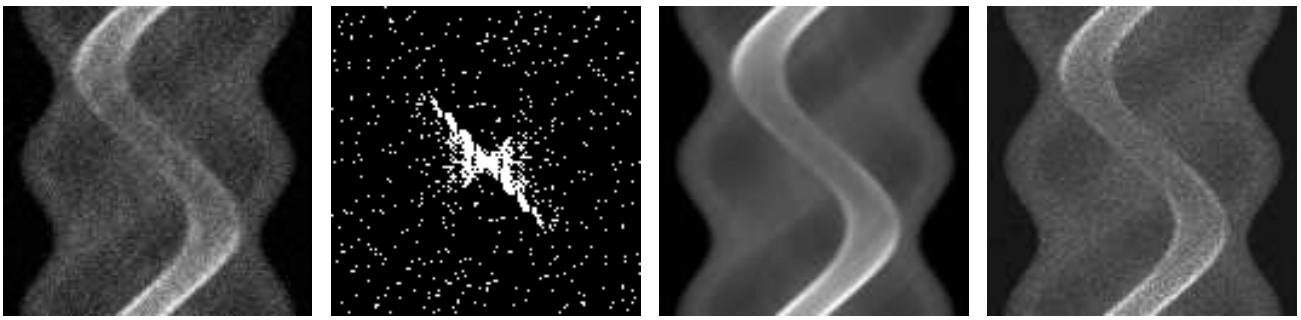

(a) (b) (c) (d)

Figure 8. Filtration result $\mathcal{W}p$ (a), its spectrum $|F\Lambda\mathcal{W}p|$ (b), $M_{200}\mathcal{W}\mathbf{p}$ (c) and $D_{200}\mathcal{W}\mathbf{p}$ (d) for $\mathcal{W} = \mathcal{A}^{simp}$.

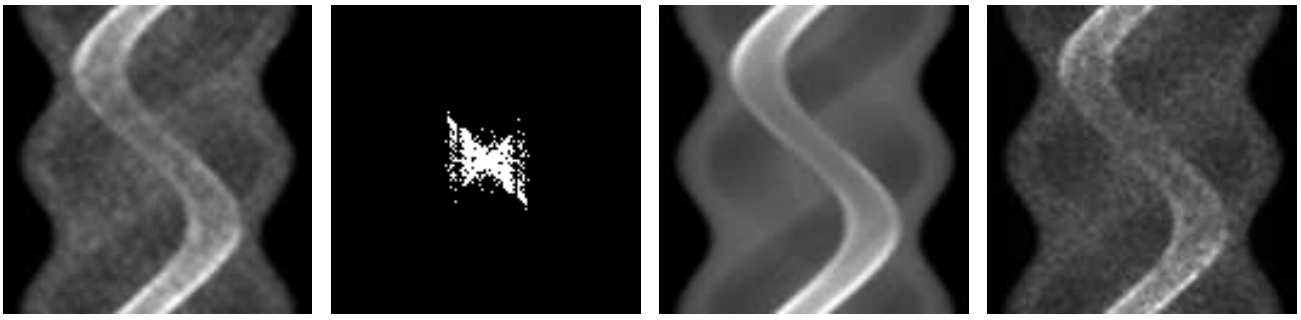

(a) (b) (c) (d)

Figure 9. Filtration result $\mathcal{W}p$ (a), its spectrum $|F\Lambda\mathcal{W}p|$ (b), $M_{200}\mathcal{W}\mathbf{p}$ (c) and $D_{200}\mathcal{W}\mathbf{p}$ (d) for $\mathcal{W} = \mathcal{A}^{sym}$.

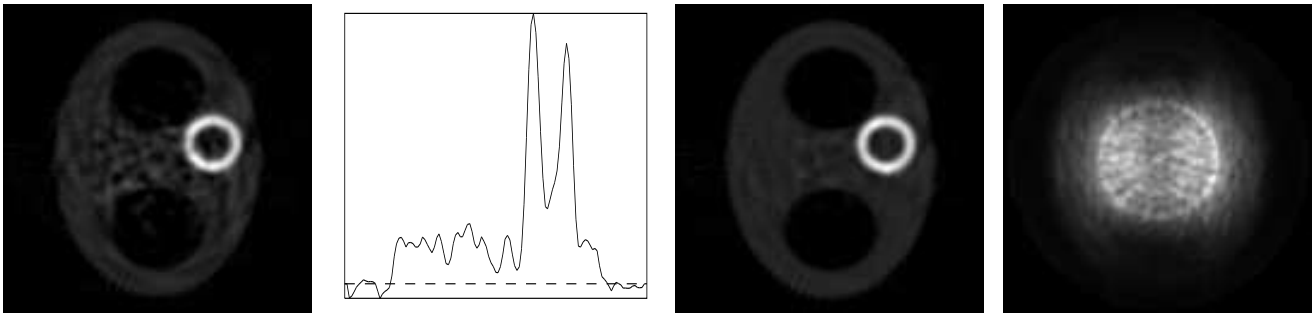

(a) (b) (c) (d)

Figure 10. Reconstruction $Cf_1 = \mathcal{N}_a \mathcal{W} p$ (a), its profile for $j = 64$ (b) and related $M_{200} Cf_1$ (c) and $D_{200} Cf_1$ (d) for $\mathcal{W} = \mathcal{W}_g^{opt}$.

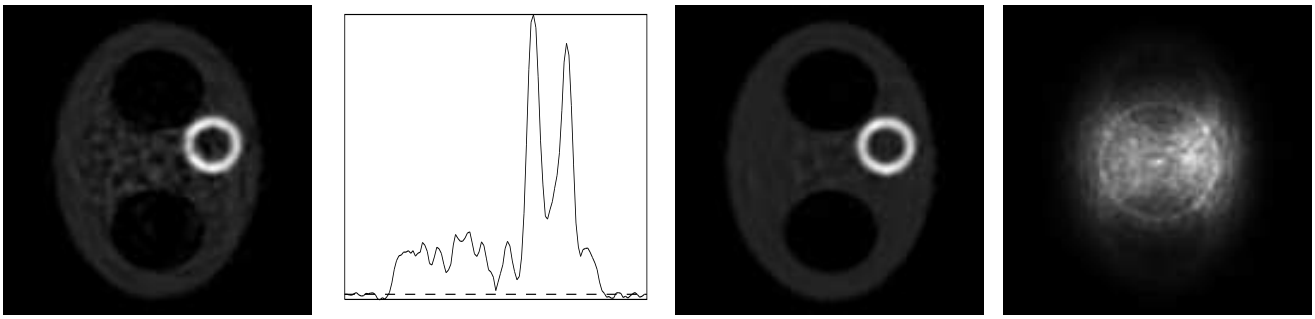

(a) (b) (c) (d)

Figure 11. Reconstruction $Cf_3 = Cf_3(\mathcal{N}_a \mathcal{W} p, a, \mathcal{W} p)$ (a), its profile for $j = 64$ (b) and related $M_{200} Cf_3$ (c) and $D_{200} Cf_3$ (d) for $\mathcal{W} = \mathcal{W}_g^{opt}$.

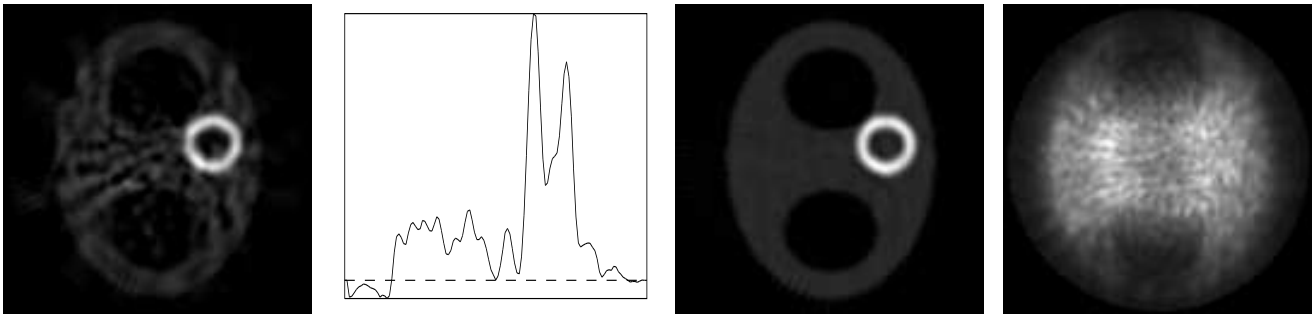

(a) (b) (c) (d)

Figure 12. Reconstruction $Cf_1 = \mathcal{N}_a \mathcal{W} p$ (a), its profile for $j = 64$ (b) and related $M_{200} Cf_1$ (c) and $D_{200} Cf_1$ (d) for $\mathcal{W} = \mathcal{W}_g^{sym}$.

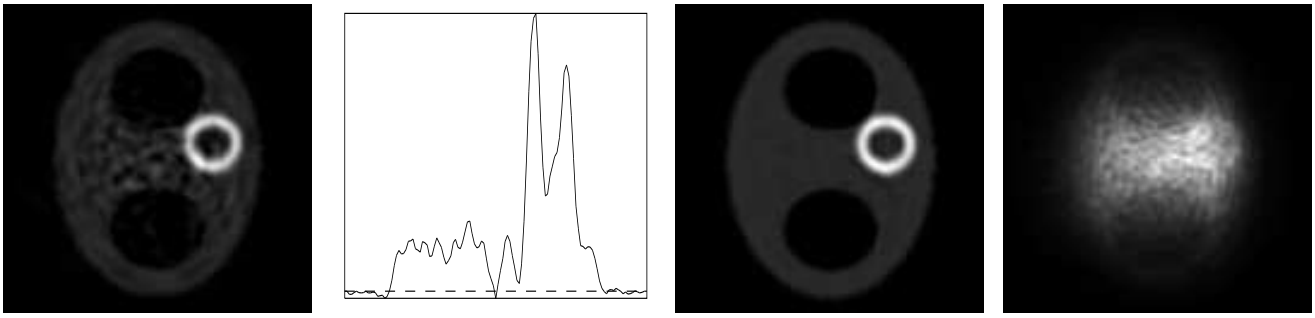

(a) (b) (c) (d)

Figure 13. Reconstruction $Cf_3 = Cf_3(\mathcal{N}_a\mathcal{W}p, a, \mathcal{W}p)$ (a), its profile for $j = 64$ (b) and related $M_{200}Cf_3$ (c) and $D_{200}Cf_3$ (d) for $\mathcal{W} = \mathcal{W}_g^{sym}$.

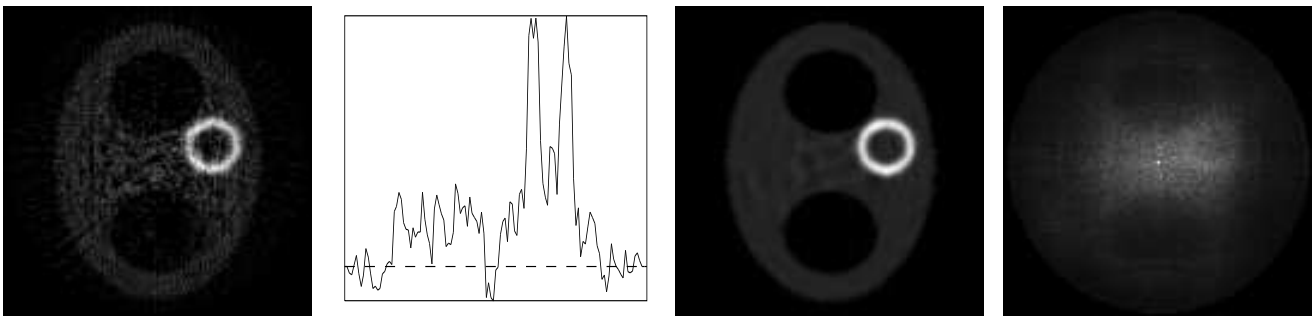

(a) (b) (c) (d)

Figure 14. Reconstruction $Cf_3 = Cf_3(\mathcal{N}_a\mathcal{W}p, a, \mathcal{W}p)$ (a), its profile for $j = 64$ (b) and related $M_{200}Cf_3$ (c) and $D_{200}Cf_3$ (d) for $\mathcal{W} = \mathcal{A}^{simp}$.

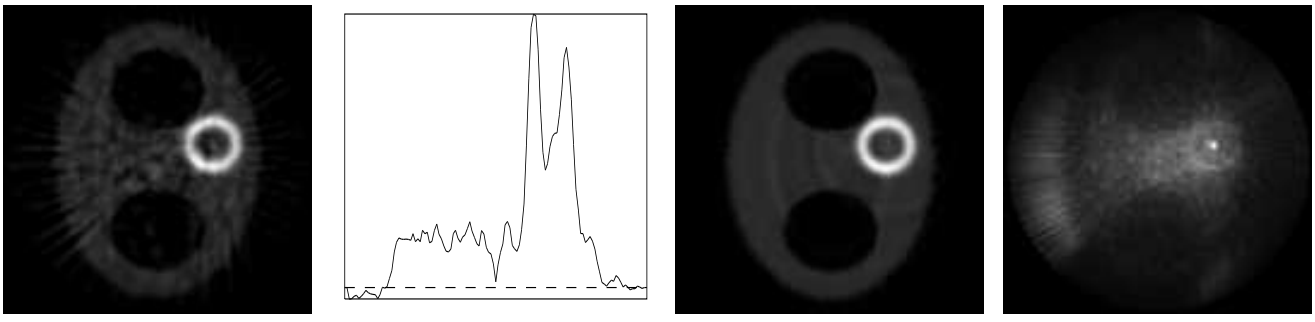

(a) (b) (c) (d)

Figure 15. Reconstruction $Cf_3 = Cf_3(\mathcal{N}_a\mathcal{W}p, a, \mathcal{W}p)$ (a), its profile for $j = 64$ (b) and related $M_{200}Cf_3$ (c) and $D_{200}Cf_3$ (d) for $\mathcal{W} = \mathcal{A}^{1d}$.

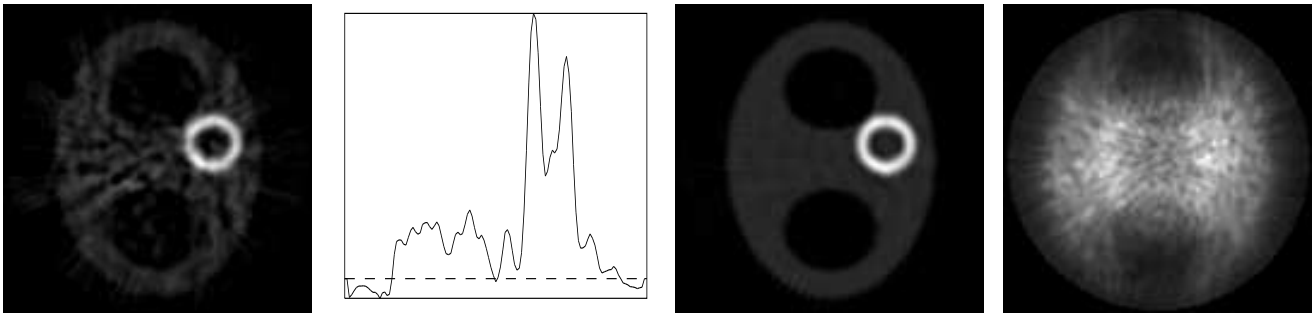

(a) (b) (c) (d)

Figure 16. Reconstruction $Cf_1 = \mathcal{N}_a \mathcal{W}p$ (a), its profile for $j = 64$ (b) and related $M_{200}Cf_1$ (c) and $D_{200}Cf_1$ (d) for $\mathcal{W} = \mathcal{A}^{sym}$.

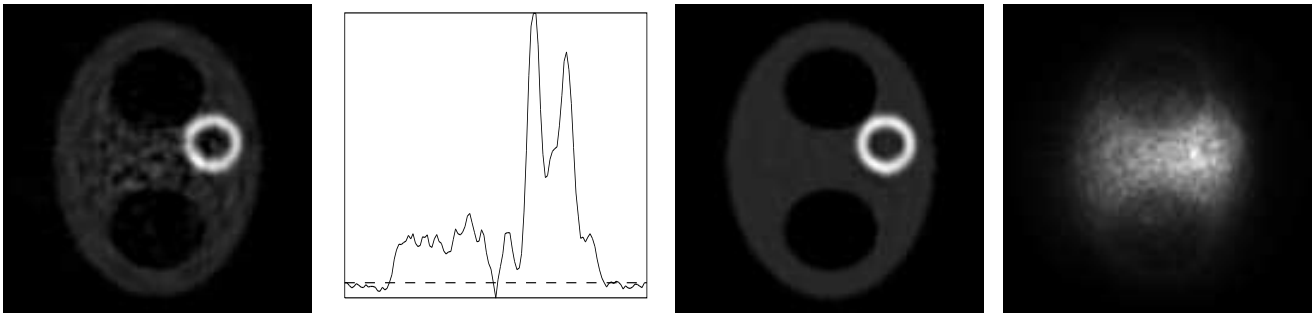

(a) (b) (c) (d)

Figure 17. Reconstruction $Cf_3 = Cf_3(\mathcal{N}_a \mathcal{W}p, a, \mathcal{W}p)$ (a), its profile for $j = 64$ (b) and related $M_{200}Cf_3$ (c) and $D_{200}Cf_3$ (d) for $\mathcal{W} = \mathcal{A}^{sym}$.

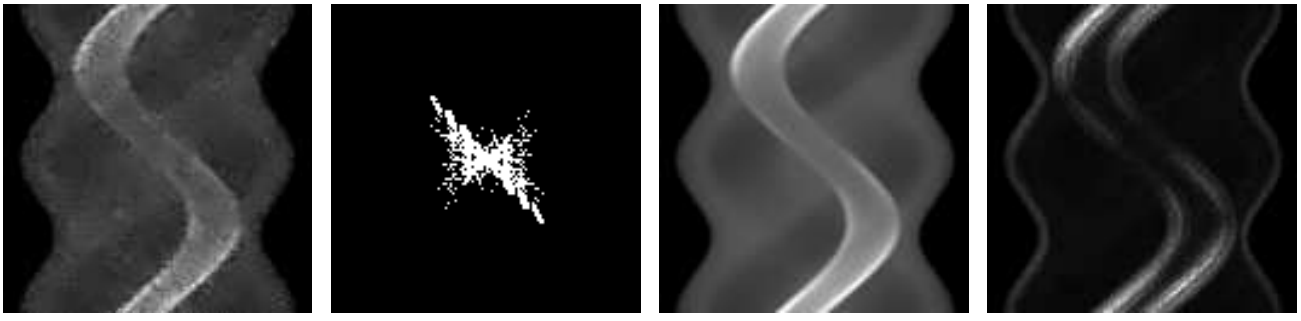

(a) (b) (c) (d)

Figure 18. Filtration result $\mathcal{W}p$ (a), its spectrum $|F\Lambda\mathcal{W}p|$ (b), $M_{200}\mathcal{W}\mathbf{p}$ (c) and $D_{200}\mathcal{W}\mathbf{p}$ (d) for $\mathcal{W} = \mathcal{A}^{sym}_{8,8}$.

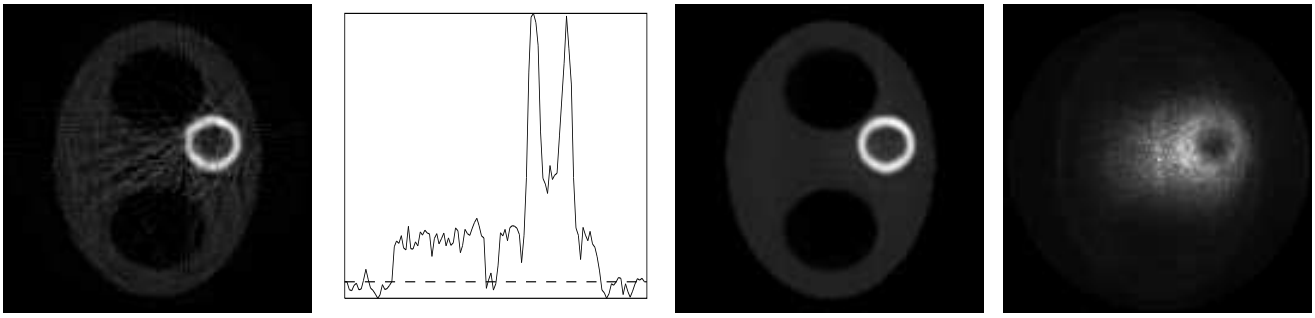

(a) (b) (c) (d)

Figure 19. Reconstruction $Cf_3 = Cf_3(\mathcal{N}_a\mathcal{W}_1 p, a, \mathcal{W}p)$ (a), its profile for $j = 64$ (b) and related $M_{200}Cf_3$ (c) and $D_{200}Cf_3$ (d) for $\mathcal{W}_1 = \mathcal{A}^{sym}$, $\mathcal{W} = \mathcal{A}^{sym}_{8,8}$.

	ζ	$e_{1,200}$	$b_{1,200}$	$d_{1,200}$	$c_{1,200}$
$\mathcal{W}_g^{opt}$	0.075	0.076	0.050	0.057	0.276
$\mathcal{W}_g^{sym}$	0.094	0.095	0.064	0.071	0.384
$\mathcal{A}^{simp}$	0.160	0.158	0.044	0.152	0.594
$\mathcal{A}^{1d}$	0.142	0.143	0.085	0.116	0.711
$\mathcal{A}^{sym}$	0.096	0.097	0.064	0.073	0.393
$\mathcal{A}_{8,8}^{sym}$	0.110	0.112	0.032	0.107	0.323
Φ_1	0.105	0.106	0.087	0.061	0.497
$\Phi_{8,8,1}$	0.089	0.091	0.047	0.078	0.315

Table 1. Numbers $\zeta = e_{1,1}$ and $e_{1,200}$, $b_{1,200}$, $d_{1,200}$, $c_{1,200}$ of (6.7), (6.11) for $\mathcal{W} = \mathcal{W}_g^{opt}$, $\mathcal{W}_g^{sym}$, $\mathcal{A}^{simp}$, $\mathcal{A}^{1d}$, $\mathcal{A}^{sym}$, $\mathcal{A}_{8,8}^{sym}$, Φ_1, $\Phi_{8,8,1}$.

	$\eta^{(1)}$	$e_{2,200}^{(1)}$	$b_{2,200}^{(1)}$	$d_{2,200}^{(1)}$	$c_{2,200}^{(1)}$
$\mathcal{W}_g^{opt}$	0.273	0.274	0.215	0.170	0.190
$\mathcal{W}_g^{sym}$	0.369	0.370	0.240	0.282	0.254
$\mathcal{A}^{simp}$	0.782	0.735	0.180	0.716	0.443
$\mathcal{A}^{1d}$	0.509	0.506	0.277	0.424	0.358
$\mathcal{A}^{sym}$	0.378	0.380	0.240	0.295	0.259
Φ_1	0.376	0.381	0.308	0.224	0.292

Table 2. Numbers $\eta^{(1)} = e_{2,1}^{(1)}$ and $e_{2,200}^{(1)}$, $b_{2,200}^{(1)}$, $d_{2,200}^{(1)}$, $c_{2,200}^{(1)}$ of (6.8), (6.12) for $\mathcal{W} = \mathcal{W}_g^{opt}$, $\mathcal{W}_g^{sym}$, $\mathcal{A}^{simp}$, $\mathcal{A}^{1d}$, $\mathcal{A}^{sym}$, Φ_1 and $P_a^{-1} = \mathcal{N}_a$.

	$\eta^{(3)}$	$e_{2,200}^{(3)}$	$b_{2,200}^{(3)}$	$d_{2,200}^{(3)}$	$c_{2,200}^{(3)}$
$\mathcal{W}_g^{opt}$	0.220	0.221	0.174	0.137	0.374
$\mathcal{W}_g^{sym}$	0.266	0.266	0.216	0.156	0.495
$\mathcal{A}^{simp}$	0.401	0.411	0.153	0.382	0.741
$\mathcal{A}^{1d}$	0.309	0.306	0.260	0.161	0.637
$\mathcal{A}^{sym}$	0.273	0.270	0.217	0.162	0.506
$\mathcal{A}_{8,8}^{sym}$	0.271	0.274	0.146	0.231	0.418
Φ_1	0.335	0.335	0.311	0.128	0.773
$\Phi_{8,8,1}$	0.252	0.255	0.185	0.175	0.438

Table 3. Numbers $\eta^{(3)} = e_{2,1}^{(3)}$ and $e_{2,200}^{(3)}$, $b_{2,200}^{(3)}$, $d_{2,200}^{(3)}$, $c_{2,200}^{(3)}$ of (6.8), (6.12) for $\mathcal{W} = \mathcal{W}_g^{opt}$, $\mathcal{W}_g^{sym}$, $\mathcal{A}^{simp}$, $\mathcal{A}^{1d}$, $\mathcal{A}^{sym}$, $\mathcal{A}_{8,8}^{sym}$ (with $\mathcal{W}_1 = \mathcal{A}^{sym}$), Φ_1, $\Phi_{8,8}$ (with $\mathcal{W}_1 = \Phi_1$) and P_a^{-1} defined by (6.20).

5. Conclusion

For 2D data with Poisson noise we found explicit formulas for the optimal space-invariant Wiener type filter with some a priori geometric restrictions on the window function; see Proposition 3.1 (of Section 3). In Section 3 some generalizations of this result are also mentioned.

Then (in Section 4) proceeding from Proposition 3.1 we (1) explain, in particular, an efficiency of the well-known (see [KDS], [SKC], [BCB], [C]) "1D" (approximately optimal) space-invariant Wiener type filtering scheme of [KDS] (with unknown object power spectrum) in SPECT and PET imaging based on the classical FBP algorithm (or its iterative use) and (2) propose also an efficient 2D (approximately optimal) space-invariant Wiener type filtration $\mathcal{A}^{sym}$ (with unknown object power spectrum) for SPECT imaging based on the generalized FBP algorithm of [Ku], [Na] (implementing the explicit formula of [No] for the nonuniform attenuation correction) and/or the classical FBP algorithm (used iteratively). In Section 6 (in Subsection 6.4) an efficient space-variant version $\mathcal{A}^{sym}_{l_1,l_2}$ of $\mathcal{A}^{sym}$ is also presented. We do not know whether the space-invariant filter $\mathcal{A}^{sym}$ in its precise form of Section 4 was mentioned in the literature. In any case our principal results concerning $\mathcal{A}^{sym}$ consist in its justification proceeding from Proposition 3.1 and in its completely space-variant version $\mathcal{A}^{sym}_{l_1,l_2}$. To our knowledge no complete generalization to the space-variant case of the filtration approach of [KDS] was mentioned in the literature before the present work.

In Section 6, the optimal, restrictedly optimal and approximately optimal space-invariant Wiener (or Wiener type) filters $\mathcal{W}^{opt}_g$, $\mathcal{W}^{sym}_g$, $\mathcal{A}^{simp}$, $\mathcal{A}^{1d}$, $\mathcal{A}^{sym}$ (mentioned in Sections 3 and 4) and the space-variant version $\mathcal{A}^{sym}_{l_1,l_2}$ of $\mathcal{A}^{sym}$ are illustrated by numerical examples in the framework of simulated SPECT imaging based on generalized and/or classical FBP algorithms. In addition, a numerical comparison (of the aforementioned filters) with the space-invariant Φ_1 and space-variant $\Phi_{l_1,l_2,1}$ data dependent filters of [GN1] and [GN2] is also given. In the numerical examples of Section 6 namely $\mathcal{A}^{sym}$ gives the best results on the level of the error-bias trade-off among all space-invariant filters with unknown object power spectrum (mentioned in the paper) and namely $\mathcal{A}^{sym}_{8,8}$ gives, in particular, the best reconstruction result Cf_3 of (6.25) on the level of the error-bias trade-off among all filters with unknown object power spectrum (mentioned in the paper); see Subsections 6.3 and 6.4.

In the present paper we do not compare yet SPECT and PET reconstructions involving Wiener type prereconstruction filtrations with maximum likelihood SPECT and PET algorithms (see [SV], [HL]). We plan to return to this comparison in subsequent work.

References

[BCB] Beis J S, Celler A and Barney J S 1995 An atomatic method to determine cutoff frequency based on image power spectrum *IEEE Trans. Nucl. Sci.* **42** 2250-2254

[BM] Bal G and Moireau P 2004 Fast numerical inversion of the attenuated Radon transform with full and partial measurements *Inverse Problems* **20** 1137-1164

[BS] Boman J and Strömberg J O 2004 Novikov's inversion formula for the attenuated Radon transform - A new approach *Journal of Geometric Analysis* **14** 185-198

[Br] Bronnikov A.V. 2000 Reconstruction of attenuation map using discrete consistency conditions *IEEE Trans. Med. Imaging* **19** 451-462

[C] Comtat C (2002) Méthodes de rétroprojection filtrée, *EPU SFPM-SFBMN, Traitement et analyse de données en médecine nucléaire*, Rouen, 13-15 mars 2002

[GB] Goodman J W and Belsher J F 1976 Fundamental limitations in linear invariant restoration of atmospherically degraded images *Imaging through Atmosphere SPIE* **75** 141-154

[GouNol] Gourion D and Noll D 2002 The inverse problem of emission tomography *Inverse Problems* **18** 1435-1460

[GJKNT] Guillement J-P, Jauberteau F, Kunyansky L, Novikov R and Trebossen R 2002 On single-photon emission computed tomography imaging based on an exact formula for the nonuniform attenuation correction *Inverse Problems* **18** L11-L19

[GN1] Guillement J-P and Novikov R G 2004 A noise property analysis of single-photon emission computed tomography data *Inverse Problems* **20** 175-198

[GN2] Guillement J-P and Novikov R G 2005 On the data dependent filtration techniques in the single-photon emission computed tomography *E-print*, https://hal.ccsd.cnrs.fr/ccsd-00009611

[GN3] Guillement J-P and Novikov R G On space-variant Wiener type filtrations in SPECT *In preparation*

[HL] Hudson H M and Larkin R S 1994 Accelerated image reconstruction using ordered subsets of projection data *IEEE Trans. Med. Imaging* **13** 601-609

[KDS] King M A, Doherty P W and Schwinger R B 1983 A Wiener filter for nuclear medicine images *Med. Phys.* **10** (6) 876-880

[Ku] Kunyansky L A 2001 A new SPECT reconstruction algorithm based on the Novikov's explicit inversion formula *Inverse Problems* **17** 293-306 (E-print, m*p*_arc/00-342)

[LM] Lewitt R M and Matej S 2003 Overview of methods for image reconstruction from projections in emission computed tomography *Proc. IEEE* **91** 1588-1611

[MN] Maeght J and Noll D 2000 Resolution in dynamic emission tomography *SIAM J. Math. Anal.* **31**(5) 1100-1120

[MNOY] Morosumi T, Nakajima M, Ogawa K and Yuta S 1984 Attenuation correction methods using the information of attenuation distribution for single photon emission CT *Med. Imaging Technol.* **2** 20-29

[MIMIKIH] Murase K, Itoh H, Mogami H, Ishine M, Kawamura M, Iio A and Hamamoto K 1987 A comparative study of attenuation correction algorithms in single photon emission computed tomography (SPECT) *Eur.J.Nucl.Med.* **13** 55-62

[Na] Natterer F 2001 Inversion of the attenuated Radon transform *Inverse Problems* **17** 113-119

[NW] Natterer F and Wübbelling F 2001 Mathematical Methods in Image Reconstruction (Philadelphia, PA: SIAM)

[No] Novikov R G 2002 An inversion formula for the attenuated x-ray transformation *Ark. Mat.* **40** 145-167 *Inverse Problems* **18** 677-700

[RL] Rattey P A and Lindgren A G 1981 Sampling the 2-D Radon Transform *IEEE Trans. Acoust. Speech Signal (Proc. ASSP-29)* 994-1002

[SKC] Shao L, Karp J S and Countryman P 1994 Practical considerations of the Wiener filtering technique on projection data for PET *IEEE Trans. Nucl. Sci.* **41** (4) 1560-1565

[SV] Shepp L A and Vardi Y 1982 Maximum likelihood reconstruction for emission tomography *IEEE Trans. Med. Imaging* **2** 113-122

[W] Wiener N 1949 Extrapolation, Interpolation, and Smoothing of stationary Times Series (New York: Wiley)